6. Mohanty SK, Arora R, Kakkar N, Kumar B. Clear cell papulosis of the skin. *Ann Diagn Pathol.* 2002;6(6):385-388.
7. Kumarasinghe SP, Chin GY, Kumarasinghe MP. Clear cell papulosis of the skin: a case report from singapore. *Arch Pathol Lab Med.* 2004;128(11): e149-e152.
8. Chong WS, Ong BH, Kumarasinghe SP. Hypopigmented papules in an Asian boy. *Pediatr Dermatol.* 2005;22(3):268-269.
9. Benouni S, Kos L, Ruggeri SY, North PE, Drolet BA. Clear cell papulosis in Hispanic siblings. *Arch Dermatol.* 2007;143(3):358-360.
10. Toker C. Clear cells of the nipple epidermis. *Cancer.* 1970;25(3):601-610.
11. Slamon DJ, Clark GM, Wong SG, Levin WJ, Ullrich A, McGuire WL. Human breast cancer: correlation to relapse and survival with amplification of the HER2/neu oncogene. *Science.* 1987;235(4785):177-182.
12. Di Tommaso L, Franchi G, Destro A, et al. Toker cells of the breast: morphological and immunohistochemical characterization of 40 cases. *Hum Pathol.* 2008;39(9):1295-1300.

Bloody Nipple Discharge in an Infant

Bloody nipple discharge (BND) is occasionally observed in women with mammary disorders such as mastitis, intraductal papilloma, or breast carcinoma. However, this phenomenon is rarely seen in infants and children; BND in infants has seldom been reported in the dermatologic literature.

Report of a Case. A 4-month-old girl was referred to our clinic with a 1-week history of unilateral BND. Her mother reported a spontaneous and intermittent BND from the infant's left breast and denied breast manipulation or trauma. The infant was healthy except for BND and had no history of taking medication. The mother had no history of drug ingestion during either pregnancy or breastfeeding.

Physical examination of the chest and nipples showed no remarkable findings such as erythema, heat, tenderness, palpable mass, or enlargement of tissue. Pressure on the areolar area resulted in a bloody discharge from the left nipple (**Figure**, A). Ultrasonography of the left breast demonstrated dilatation of the retroareolar mammary ducts (Figure, B). The results of a blood cell count and coagulation tests were within the normal range. Culture of the bloody discharge revealed no bacterial growth. Cytologic examination of the secretion showed abundant erythrocytes but no other atypical cells. Based on these findings, bacterial infection and breast carcinoma were ruled out as a cause of the BND, and we decided to observe her without any treatment.

Comment. Bloody nipple discharge in infants, first described by Berkowitz and Inkelis,[1] occurs unilaterally or bilaterally in both sexes. Most patients older than 1 year show a palpable mass or breast enlargement, whereas infantile patients sometimes present with a normal appearance.[2] In laboratory examinations, coagulation test results and serum hormone levels are usually found to be normal, and culture of the discharge is usually negative.[2]

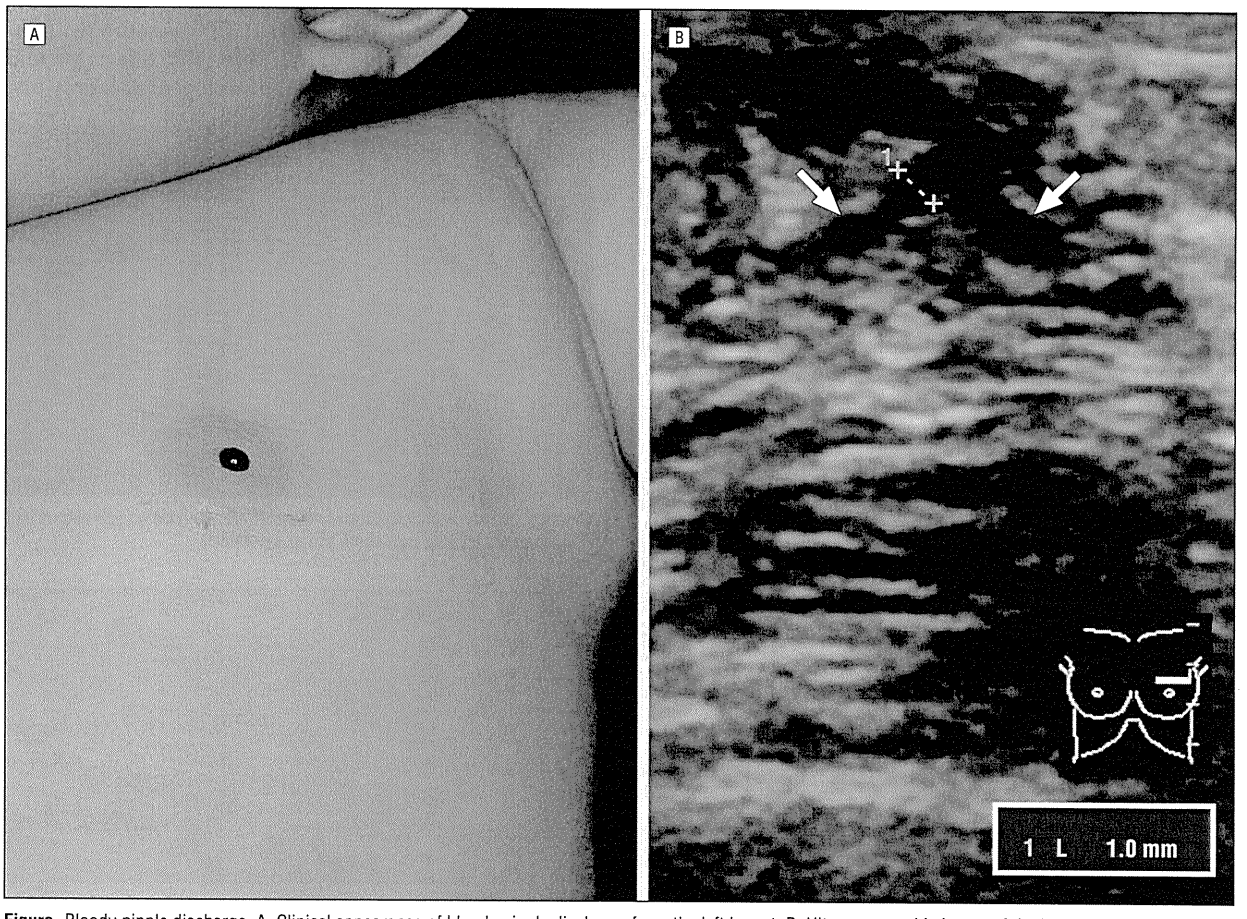

Figure. Bloody nipple discharge. A, Clinical appearance of bloody nipple discharge from the left breast. B, Ultrasonographic image of the left breast showing dilatation of the subareolar mammary ducts (arrows).

Histopathologically, mammary duct ectasia, a benign lesion characterized by dilated ducts surrounded by fibrosis and inflammation, has been proven in more than half of childhood BND cases with palpable masses treated surgically.[2] Mammary duct ectasia has also been detected by ultrasonography even in infantile cases with nonpalpable masses.[3,4] Underlying breast carcinoma should definitely be ruled out when we see patients with BND, but to our knowledge, it has never been reported in infants.[4,5] From these data, mammary duct ectasia is the most likely cause of BND in infants and children, although the specific cause of duct ectasia remains unclear.

To our knowledge, all but 1 of the reported BND cases in infants has achieved spontaneous resolution within 9 months.[3-5] The 1 case that did not resolve spontaneously was treated surgically. These facts suggest that BND in infants is a benign and self-limiting condition. Therefore, invasive intervention, including biopsy, should be avoided, especially in girls, because even minimal operative injury to the breast bud may produce severe tissue damage resulting in functional disability and persistent disfigurement.[4,5] Noninvasive investigations such as culture of the discharge and ultrasonographic evaluation are recommended as well as a careful physical examination and close clinical follow-up. Only if ultrasonography reveals a mass or abnormality other than mammary duct ectasia, or if the discharge persists for more than 9 months, should further investigations, including invasive interventions, be considered.[5]

Hideyuki Ujiie, MD
Masashi Akiyama, MD, PhD
Rinko Osawa, MD
Satoru Shida, MD, PhD
Satoru Aoyagi, MD, PhD
Hiroshi Shimizu, MD, PhD

Correspondence: Dr Ujiie, Department of Dermatology, Hokkaido University Graduate School of Medicine, North 15 W 7, Kita-ku, Sapporo 060-8638, Japan (h-ujiie@med.hokudai.ac.jp).
Financial Disclosure: None reported.

1. Berkowitz CD, Inkelis SH. Bloody nipple discharge in infancy. *J Pediatr*. 1983; 103(5):755-756.
2. Imamoglu M, Cay A, Reis A, Ozdemir O, Sapan L, Sarihan H. Bloody nipple discharge in children: possible etiologies and selection of appropriate therapy. *Pediatr Surg Int*. 2006;22(2):158-163.
3. Weimann E. Clinical management of nipple discharge in neonates and children. *J Paediatr Child Health*. 2003;39(2):155-156.
4. De Praeter C, De Coen K, Vanneste K, Vanhaesebrouck P. Unilateral bloody nipple discharge in a two-month-old male. *Eur J Pediatr*. 2008;167(4):457-459.
5. Kelly VM, Arif K, Ralston S, Greger N, Scott S. Bloody nipple discharge in an infant and a proposed diagnostic approach. *Pediatrics*. 2006;117(4):e814-e816.

Acute Generalized Exanthematous Pustulosis Caused by Rifabutin

Acute generalized exanthematous pustulosis (AGEP), first named by Beylot et al[1] in 1980, is a clinical reaction pattern that is principally drug induced.[2,3] Its incidence is probably underestimated because many cases are either unrecognized or confused with pustular psoriasis.[3] We report herein a case of AGEP caused by rifabutin, an antituberculous agent.

Report of a Case. A 58-year-old man with hypertension, coronary artery disease, and schizophrenia was admitted to our hospital for cervical nontuberculous mycobacterial lymphadenitis. He had a history of drug allergy to trimethoprim-sulfamethoxazole presenting as a generalized nonpustular exanthematous eruption. After 10 days of treatment with rifabutin, he developed a fever with temperatures up to 38°C accompanied by numerous nonfollicular sterile pustules on widespread edematous erythema over the trunk and all extremities without mucous membrane involvement (**Figure 1**).

Laboratory examinations revealed leukocytosis with left shift and mild eosinophilia. (The white blood cell count was 11200/μL; neutrophil-bands, 12%; eosinophil-bands, 7%; to convert white blood cells to 10^9/L, multiply by 0.001.) Histopathologic evaluation showed spongiform subcorneal pustules with a predominance of neutrophils and eosinophils and papillary dermal edema with perivascular inflammatory cell infiltrate (**Figure 2**).

Rifabutin treatment was discontinued, and intravenous hydrocortisone, 100 mg, was administered every 6 hours. The pustules resolved rapidly with generalized desquamation and have not recurred. Acute generalized exanthematous pustulosis was confirmed by validation score of the EuroSCAR study group.[2]

Comment. More than 90% of AGEP cases are drug induced, mainly by antibiotics, especially ß-lactams and macrolides.[2,3] Our patient had no personal or family his-

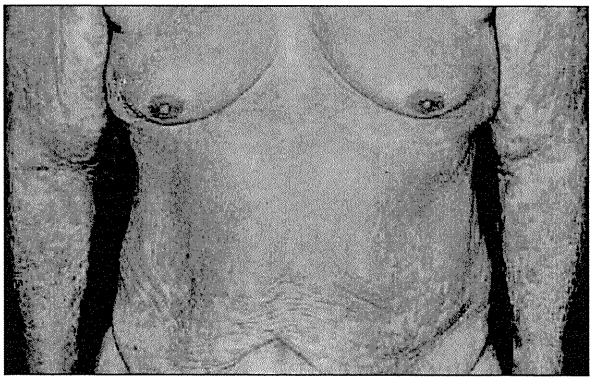

Figure 1. Numerous nonfollicular pinhead sterile pustules on edematous and erythematous plaques over trunk and all extremities.

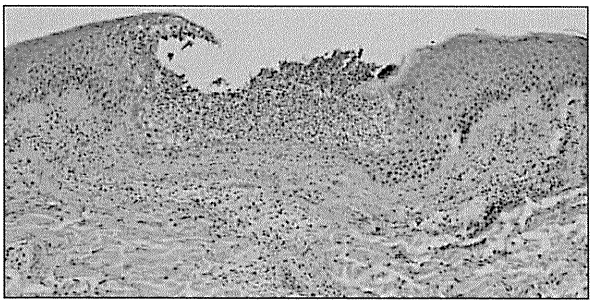

Figure 2. Spongiform subcorneal pustule with mixed neutrophils and eosinophils and a focal necrosis of keratinocytes in the epidermis (hematoxylin-eosin, original magnification ×100).

Glycosylation Specific for Adhesion Molecules in Epidermis and Its Receptor Revealed by Glycoform-focused Reverse Genomics*[S]

Rie Uematsu‡, Yasuro Shinohara‡§, Hiroaki Nakagawa‡, Masaki Kurogochi‡, Jun-ichi Furukawa‡, Yoshiaki Miura‡, Masashi Akiyama¶, Hiroshi Shimizu¶, and Shin-Ichiro Nishimura‡‖

Glycosylation of proteins greatly affects their structure and function, but traditional genomics and transcriptomics are not able to precisely capture tissue- or species-specific glycosylation patterns. We describe here a novel approach to link different "omics" data based on exhaustive quantitative glycomics of murine dermis and epidermis. We first examined the dermal and epidermal *N*-glycome of mouse by a recently established glycoblotting technique. We found that the Galα1–3Gal epitope was solely expressed in epidermis tissue and was preferentially attached to adhesion molecules in a glycosylation site-specific manner. Clarified glycomic and protemic information combined with publicly available microarray data sets allowed us to identify galectin-3 as a receptor of Galα1–3Gal epitope. These findings provide mechanistic insight into the causal connection between the genotype and the phenotype seen in α3GalT-1-deficient mice and transgenic mice expressing endo-β-galactosidase C. Because humans do not possess the Galα1–3Gal structure on their tissues, we further examined the human dermal and epidermal *N*-glycome. Comparative glycomics revealed that the GalNAcβ1–4GlcNAc (*N,N'*-diacetyllactosediamine) epitope, instead of the Galα1–3Gal epitope, was highly expressed in human epidermis. ***Molecular & Cellular Proteomics 8:232–244, 2009.***

Posttranslational protein glycosylation changes the biological and physical properties of glycoconjugates, which include functions as signals or ligands to control their distribution, antigenicity, metabolic fate, stability, and solubility (1). Cells in the epidermis, which forms a major part of the epithelial barrier, undergo desquamation and are continuously being renewed (2), a process that requires changes in adhesion. Because glycoproteins are often involved in adhesion between cells and their extracellular matrices, the glycoproteome of the epidermis may therefore provide new insight into the functional roles of protein glycosylation. Mammalian epidermal glycoconjugates have mostly been studied histochemically using lectins (3) or monoclonal antibodies (4). Although these studies revealed that the cell surfaces of keratinocytes in the epidermis contain numerous glycoconjugates, these approaches cannot provide detailed structural information about the oligosaccharides or their carrier proteins.

We previously clarified the quantitative glycomic profile of murine dermis and epidermis using novel aminooxy-based isotope tags and MALDI-TOF MS analysis (5), which revealed distinct features of the *N*-glycosylation profile of dermis and epidermis. We found that murine epidermal glycoproteins have a high abundance of high mannose-type oligosaccharides, and the striking roles of lysosomal enzymes in epidermis during lipid remodeling and desquamation were further discussed. This study was the first to demonstrate the usefulness of quantitative gross *N*-glycan profiling for performing systematic glycoform-focused proteomics. To advance and accelerate this approach, we recently established a novel technology platform for large scale quantitative glycomics based on the glycoblotting technique (6–8). In this method, glycans derived from biological samples are selectively captured onto novel high density hydrazide beads (BlotGlyco H) for highly efficient purification of oligosaccharides from complex biological samples. The captured oligosaccharides are subjected to on-bead methyl esterification to stabilize sialic acid(s) for the simultaneous quantitation of neutral and sialylated oligosaccharides by MALDI-TOF MS and are finally recovered as arbitrary derivatives by imine exchange chemistry.

In the current study, we first used this newly established glycoblotting technique to re-examine both the neutral and sialylated *N*-glycome of murine dermis and epidermis. We detected 75 oligosaccharides, more than twice the amount detected previously when sialic acids were removed, thus enabling us to perform a more detailed comparison of tissue-specific *N*-glycosylation profiles. We found that the expression of oligosaccharides containing the Galα1–3Gal epitope was only detected in epidermis, although many non-reducing terminal epitopes tend to vanish in epidermis. Tracing from

From the ‡Graduate School of Advanced Life Science, Hokkaido University, Sapporo 001-0021, Japan and ¶Department of Dermatology, Hokkaido University Graduate School of Medicine, Sapporo 060-8638 Japan

Received, April 1, 2008, and in revised form, August 29, 2008
Published, MCP Papers in Press, September 29, 2008, DOI 10.1074/mcp.M800145-MCP200

the glycome back to the proteome and transcriptome allowed us to identify a group of proteins that carry Galα1–3Gal epitope and a receptor that can recognize Galα1–3Gal epitope. The glycans identified in mice epidermis could account for the phenotypes observed in transgenic mice expressing endo-β-galactosidase C. Finally human epidermal glycomics was evaluated aiming to address the question of whether any alternative glycan structures play a role similar to that of the Galα1–3Gal epitope in murine epidermis.

EXPERIMENTAL PROCEDURES

Skin Samples and Tissue Preparation—Male hairless mice (Hos/HR-1) were obtained from Sankyo Labo Service (Tokyo, Japan). They were fed a standard mouse diet and water *ad libitum*. Full thickness skin samples were taken from the dorsal area of 7–12-week-old animals. Animal experiments were performed according to the respective regulatory standards of Hokkaido University. Normal human skin samples were obtained from patients during resection operations. The medical ethics committee at Hokkaido University approved all of the described studies, and all of the participants gave their written informed consent. After removal of excess subcutaneous fat from the skin samples, the epidermis was peeled from the dermis by heat separation at 60 °C for 30 s. The epidermis and dermis were minced and heated at 90 °C for 10 min in 10 mM ammonium bicarbonate, then defatted as described by Bligh and Dyer (9), and lyophilized.

N-Glycan Release—*N*-Glycans were released from tissues in previously optimized conditions (10) with minor modifications. Each defatted and lyophilized tissue (equivalent to 3 mg) was suspended in 0.02% 1-propanesulfonic acid, 2-hydroxy-3-lauramido in 10 mM ammonium bicarbonate; reduced with DTT; *S*-carbamoylmethylated; and digested with trypsin (Sigma). Following deglycosylation by treatment with peptide-*N*-glycosidase F (PNGase F;[1] Hoffmann-La Roche), the samples were digested with Pronase (Calbiochem). The supernatant was evaporated to dryness and redissolved in 120 μl of 10 mM ammonium bicarbonate.

N-Glycan Purification and Derivatization—*N*-Glycans in the de-*N*-glycosylated sample were purified and labeled by using a previously described method (7). Briefly 20-μl aliquots of epidermis and dermis samples were applied to a polymer displaying hydrazide functionality at high density (BlotGlyco H), 180 μl of 2% acetic acid in acetonitrile was added, and the released *N*-glycans were captured via hydrazone linkage by incubation at 80 °C for 45 min. After the beads were washed with 2 M guanidine hydrochloride in ammonium bicarbonate, H_2O, and 1% triethylamine in methanol, 10% acetic anhydride in methanol was added, and the solution was incubated at room temperature for 30 min to cap the residual hydrazide groups. Following the washing of the beads with 10 mM hydrochloric acid, methanol, and dioxane, the sialic acids were methyl esterified by incubation at 60 °C for 60 min with 100 mM 3-methy-1-*p*-tolyltriazene in dioxane. The beads were washed with dioxane, H_2O, methanol, and H_2O, and then 20 μl of 20 mM N^{α}-((aminooxy)acetyl)tryptophanylarginine methyl ester (aoWR) and 180 μl of 2% acetic acid in acetonitrile were added. The solutions were heated at 80 °C for 45 min to transfer the glycans captured on the beads to aoWR, and the glycans were eluted with H_2O. To remove the excess aoWR, an aliquot of each sample was applied to a MassPREP™ hydrophilic interaction chromatography μElution Plate (Waters, Milford, MA) according to the manufacturer's instructions with minor modifications. Following washing with 1% acetic acid, the wells were equilibrated with 1% acetic acid in 95% acetonitrile. After the addition of each sample, the wells were washed with equilibration solution and eluted with 1% acetic acid in 5% acetonitrile.

N-Glycan Profiling by MALDI-TOF—Each purified aoWR-derivatized sample was dried and diluted with 10 μl of 2,5-dihydroxybenzoic acid (DHB; 10 mg/ml in 30% acetonitrile; Bruker Daltonics, Bremen, Germany), and an aliquot (1 μl) was deposited on the stainless steel target plate. The aoWR derivatized samples were analyzed to elucidate the relative quantities of the different oligosaccharides present in each tissue. MALDI-TOF data were obtained using an Ultraflex time-of-flight mass spectrometer (Bruker Daltonics) equipped with a LIFT-TOF/TOF unit controlled by the FlexControl 2.2 software package. All of the spectra were obtained using the reflectron mode with an acceleration voltage of 25 kV, a reflector voltage of 26.3 kV, and a pulsed ion extraction of 160 ns in the positive ion mode. The results were obtained by accumulating the signals of 1,000 laser shots. The signal intensity of each mass was automatically calculated by FlexAnalysis 2.0. Estimations of *N*-linked type oligosaccharide structures were obtained by entering the peak masses into the GlycoMod Tool (Swiss Institute of Bioinformatics) and GlycoSuite (Proteome Systems).

Neutral N-Glycan Profiling by the Two-dimensional Mapping Technique—Each sample was also analyzed by derivatization with 2-aminopyridine (PA) followed by the two-dimensional mapping technique as described previously (11, 12). Briefly *N*-glycans in the de-*N*-glycosylated sample were purified by gel filtration and derivatized with PA and sodium cyanoborohydride. After removal of unreacted PA by Sephadex G-15 (GE Healthcare), the PA-oligosaccharides were further purified by collecting the elution from amide-80 (4.6 × 250 mm, Tosoh, Tokyo, Japan) using HPLC. The mixture of PA-oligosaccharides was applied to an octadecylsilyl silica (ODS; 6 × 150 mm, Shimadzu, Kyoto, Japan) HPLC column, and the elution times of the individual peaks were normalized with reference to the PA-derivatized isomalto-oligosaccharides of polymerization degree 4–20 and represented by GU (ODS). Then individual fractions separated on the ODS column were applied to the amide-80 column. Similarly the retention time of the individual peaks on the amide-80 column were represented by GU (amide). Thus, a given compound from these two columns provided a set of GU (ODS) and GU (amide) values, which corresponded to coordinates of the two-dimensional sugar map. By comparison with the coordinates of reference PA-oligosaccharides, the *N*-glycans from skin were identified. Identification was confirmed by co-chromatography with a candidate reference on the columns and sequential exoglycosidase digestion. Molar ratios of *N*-glycans were calculated from the individual peak areas.

MALDI-TOF/TOF MS of PA-derivatized N-Glycans Using the Matrix-dependent Selective Fragmentation (MDSF) Method—Some of the PA-derivatized *N*-glycans also were analyzed by MALDI-LIFT-TOF/TOF MS using MDSF according to the procedure described previously (13, 14). α-Cyano-4-hydroxycinnamic acid (Bruker Daltonics) was prepared as a saturated solution in 3:1 (v/v) acetonitrile/water. The desalted PA-derivatized *N*-glycan samples were dissolved in water, applied on the target spot of the stainless steel target plate, mixed with 1 μl of matrix solution (either 2,5-dihydroxybenzoic acid or

[1] The abbreviations used are: PNGase F, peptide-*N*-glycosidase F; ConA, concanavalin A; aoWR, N^{α}-((aminooxy)acetyl)tryptophanylarginine methyl ester; LacdiNAc, *N*,*N*′-diacetyllactosediamine (GalNAcβ1–4GlcNAc); PA, 2-aminopyridine; ODS, octadecylsilyl silica; MDSF, matrix-dependent selective fragmentation; Ah, anthraniloyl hydrazine; SPR, surface plasmon resonance; Fuc, fucose; M2, $Man_2GlcNAc_2$; M3, $Man_3GlcNAc_2$; M3F, $Man_3GlcNAc_2Fuc$; M4, $Man_4GlcNAc_2$; NeuAc, *N*-acetylneuraminic acid; NeuGc, *N*-glycolylneuraminic acid; MHC, major histocompatibility complex; Susd 2, sushi domain-containing protein-2; α3GalT, α1,3-galactosyltransferase; GU, glucose unit.

α-cyano-4-hydroxycinnamic acid), and dried at room temperature. All measurements were performed using an Ultraflex TOF/TOF mass spectrometer equipped with a reflector and controlled by the FlexControl 2.2 software package (Bruker Daltonics). In MALDI-TOF MS reflector mode, ions generated by a pulsed UV laser beam (nitrogen laser, λ = 337 nm, 5 Hz) were accelerated to a kinetic energy of 23.5 kV. Metastable ions generated by laser-induced decomposition of the selected precursor ions were analyzed without any additional collision gas. In MALDI-LIFT-TOF/TOF mode, precursor ions were accelerated to 8 kV and selected in a timed ion gate. The fragments were further accelerated by 19 kV in the LIFT cell, and their masses were analyzed after the ion reflector passage. Masses were automatically annotated by using the FlexAnalysis 2.2 software package.

Preparation of Glycopeptides—Defatted and lyophilized murine epidermis (30–50 mg) was dissolved in a solution of 7 M guanidine hydrochloride, 0.5 M Tris-HCl, pH 8.5, and 10 mM EDTA; reduced with DTT; and *S*-carbamidomethylated. The alkylated proteins were dialyzed against 10 mM ammonium bicarbonate and digested with trypsin. The digested proteins were applied to a concanavalin A (ConA)-agarose (Seikagaku Co., Tokyo, Japan) column equilibrated with a solution of 150 mM NaCl, 1 mM $MgCl_2$, 1 mM $CaCl_2$, and 10 mM Tris-HCl buffer, pH 7.5. After the column was washed with equilibrated buffer, the glycopeptides carrying biantennary complex-type oligosaccharides were eluted with buffer containing 10 mM methyl α-glucopyranoside. The eluted glycopeptides were then separated on an ODS column using HPLC with a linear gradient of acetonitrile (0–32%) in 0.1% formic acid. Chromatography was carried out at a flow rate of 1 ml/min at room temperature and was monitored at 214 nm. The glycopeptide mixture was separated into 100 fractions and dried with a centrifugal vacuum concentrator. The fractionated glycopeptides were dissolved in 10 μl of 30% acetonitrile. A portion (1 μl) of each fraction was deglycosylated by PNGase F and dissolved in the matrix solution.

Glycopeptide Identification by MALDI-TOF/TOF—Each fraction with and without PNGase F treatment was mixed with 2,5-dihydroxybenzoic acid (10 mg/ml in 30% acetonitrile) and then applied to the MALDI target plate. MALDI-TOF and MALDI-TOF/TOF data were obtained using an Ultraflex time-of-flight mass spectrometer as above. For fragmentation ion analysis in the TOF/TOF mode, precursors were accelerated to 8 kV and selected in a timed ion gate. Fragment ions generated by laser-induced decomposition of the precursor were further accelerated by 19 kV in the LIFT cell, and their masses were analyzed after passing the ion reflector. Masses were automatically annotated by using FlexAnalysis 2.0. External calibration of MALDI-TOF MS was carried out using singly charged monoisotopic peaks and fragments of a mixture of human angiotensin II (*m/z* 1046.542; Bruker Daltonics), bombesin (*m/z* 1619.823; Bruker Daltonics), and adrenocorticotropic hormone-(18–39) (*m/z* 2465.199; Bruker Daltonics).

Protein Identification by Database Search—Peak lists were generated from the MS/MS spectra using Bruker FlexAnalysis (Version 2.0) and were processed by the MASCOT™ (Version 2.1, Matrix Science, London, UK) search algorithm to assign peptides based on the Mass Spectrometry Protein Sequence Database (MSDB database updated February 27, 2005, 1,942,918 sequences), a database containing 75,031 mouse genome sequences. The database was searched for tryptic peptides with up to one miscleavage and a mass tolerance for the precursor ions of 1.2 Da and for the fragment ions of 2.0 Da. All cysteine residues were treated as being carbamidomethylated. Deamidation of asparagines caused by deglycosylation was considered. We first screened the candidate peptides with probability-based MOWSE (molecular weight search) scores that exceeded their thresholds ($p < 0.05$) and with MS/MS signals for y- or b-ions >5. If the peptide did not contain the consensus tripeptide sequence for *N*-linked glycosylation (N*X*(S/T)) the data were eliminated regardless of the matching score. In total, 14 sets of MS/MS data were obtained.

Determination of the Relative Quantities of the Microheterogeneous Glycoforms Present at Each N-Glycan Binding Site—Following the fractionation of ConA-bound fractions (eluted with buffer containing 10 mM methyl α-glucopyranoside or 100 mM methyl α-mannopyranoside), each fraction was further analyzed by reversed-phase chromatography as described previously (5). The relative quantitation of the microheterogeneity of different glycoforms present at a particular *N*-glycan binding site was determined by comparing the signal intensities upon mixing the same volume from each successive fraction that contained the same peptide backbone.

Purification of Oligosaccharide Having Galα1–3Gal Epitope and Labeling with Biotin—Purification of oligosaccharide having the Galα1–3Gal epitope and its labeling with biotin were performed as described previously (7). Briefly alkylated and dialyzed murine epidermal proteins were digested with trypsin/PNGase F and were subjected to glycoblotting as described above. The blotted oligosaccharides were recovered as anthraniloyl hydrazine (Ah) derivatives, which are fluorogenic and suitable for chromatographic separation. Ah-derivatized oligosaccharides were subjected to ConA immobilized affinity chromatography and normal-phase HPLC according to the procedure described previously (15). Purified oligosaccharides (100 pmol) were dissolved in 2% acetic acid in 98% acetonitrile and were incubated with aminooxy biotin (Biotium, Inc.) (2 nmol) to promote the conversion of Ah derivatives to biotin derivatives. To remove the excess aminooxy biotin, an aliquot of samples was applied to an amide-80 column.

Surface Plasmon Resonance Analysis—The aminooxy-labeled oligosaccharide (10 pmol) was introduced onto a streptavidin preimmobilized sensor surface (sensor chip SA-5 (BIACORE AB, Uppsala, Sweden)). Recombinant murine galectin-3 and -7 (R&D Systems, Inc.) were purified with Superdex 200 10/300 GL (GE Healthcare) to remove excess carrier protein. Interactions were monitored by surface plasmon resonance (SPR) using a BIACORE 2000 system (BIACORE AB) as described previously (16). The reference flow cell sensorgram (determined by injection over a blank surface) was subtracted from the corresponding sensorgrams to abolish base-line drift, bulk, and nonspecific interaction contributions.

RESULTS AND DISCUSSION

Gross N-Glycan Profiling of Murine Dermis and Epidermis—We analyzed the murine dermal and epidermal *N*-glycomes using a recently established glycoblotting technique (7) that utilizes a polymer displaying high density hydrazide functionality (BlotGlyco H) coupled with solid-phase methyl esterification of sialic acids and subsequent tag conversion by aoWR, a labeling reagent (MS probe) for highly sensitive MALDI-TOF MS. As shown in Fig. 1, the MALDI-TOF MS spectra obtained from each sample differed substantially; the epidermal glycome tended to be of smaller molecular size than dermal glycome. We detected 75 oligosaccharides in either dermis or epidermis, more than twice the number detected previously when sialic acids were removed (5). This great increase is attributable not only to the addition of a variety of sialylated species but also to improved detection sensitivity from the drastically improved signal-to-noise ratio obtained with the glycoblotting technique because of its extremely high purification power. The structure and relative abundance of each detected oligosaccharide are summarized

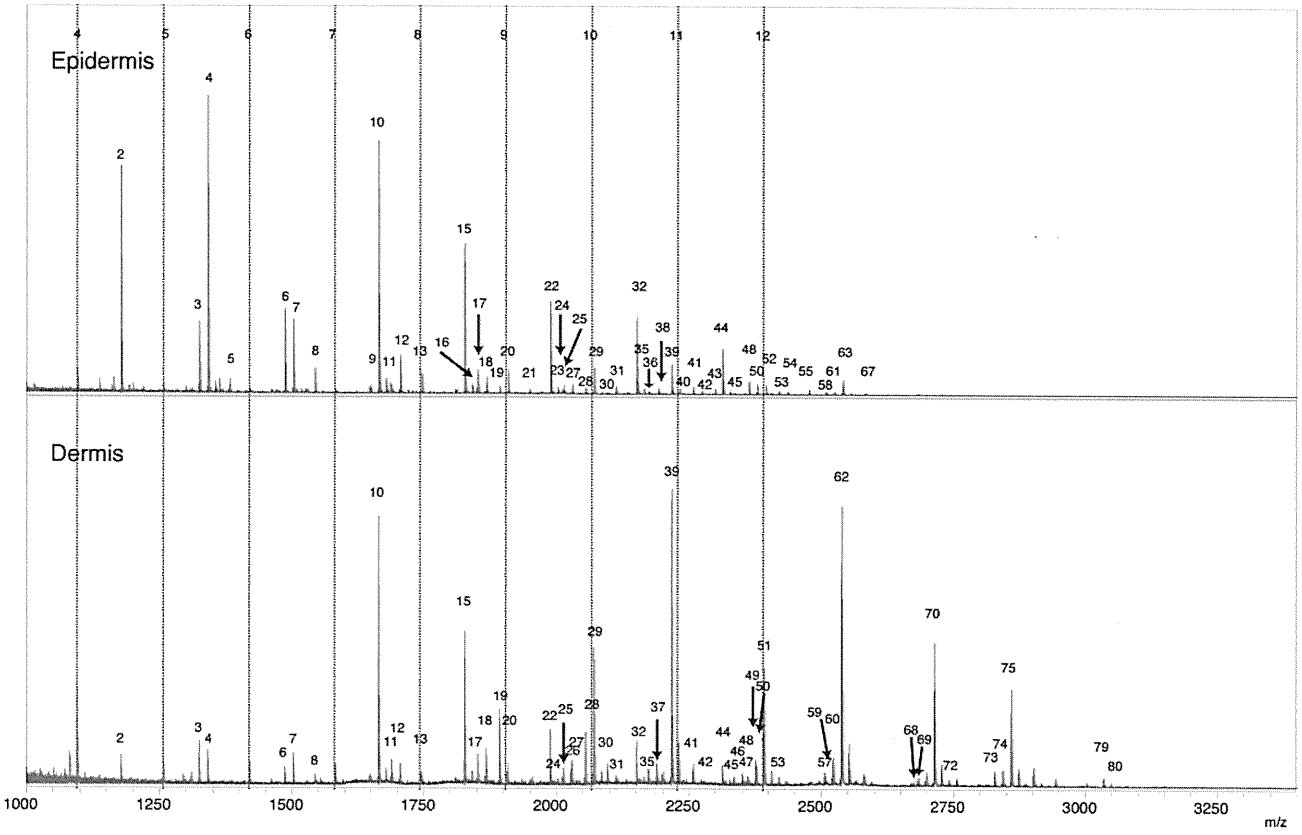

FIG. 1. **MALDI-TOF spectra showing the *N*-glycan profiles of murine skin glycoproteins.** *N*-Glycans derived from skin tissues were derivatized with aoWR(H). The putative compositions of the *numbered* oligosaccharide signals are shown in Table I. *Dotted lines* with *numbers* were putatively assigned to be hexose oligomers ($(Hex)_{4-12}$).

in Table I. We quantified the relative abundance of each type of structure in the observed oligosaccharides (Fig. 2). High mannose-type oligosaccharides, including $Man_2GlcNAc_2$ (M2), $Man_3GlcNAc_2$ (M3), $Man_3GlcNAc_2Fuc$ (M3F), and $Man_4GlcNAc_2$ (M4) were more highly expressed in epidermis than in dermis (Fig. 2*a*). The relative abundance of M2, M3, M3F, and M4, which are considered to be degraded products according to the well characterized *N*-glycan biosynthesis (17), was much higher in epidermis than in dermis (Fig. 2*b*, "*Others*") in good agreement with our previous report (5).

Sialylated species were scarcely observed in epidermis, whereas ~40% of dermal *N*-glycans were found to be sialylated (Fig. 2*a*). In mice, the sialylated species include both *N*-acetylneuraminic acid (NeuAc) and *N*-glycolylneuraminic acid (NeuGc), but NeuGc was the major sialic acid form (Fig. 2*c*). The relative abundance of oligosaccharides having one or more fucose residues was also substantially lower in epidermis than in dermis; fewer than 30% of epidermal oligosaccharides were modified with fucose, whereas 50–60% of dermal oligosaccharides were fucosylated (Fig. 2*d*). The relatively smaller molecular size observed for the epidermal *N*-glycome may in part be attributable to decreased sialylation as well as fucosylation. This finding, in conjunction with the marked increase of M2, M3, M4, and their fucosylated analogues in epidermis, suggests that glycoforms of epidermal glycoproteins are often trimmed by several glycosidases. These observations most likely reflect the unique epidermal environment, which is rich in degradation enzymes, including various glycosidases, because of the desquamation of living cells (18). Thus although many non-reducing terminal epitopes vanished, interestingly the expression of oligosaccharides containing the Galα1–3Gal epitope was only detected in epidermis (Fig. 2*e*). The presence of the Galα1–3Gal epitope in mice epidermis was predicted from the histochemical studies using *Griffonia simplicifolia*-I (GS-I), a lectin known to bind to the Galα1–3Gal epitope (19), although the histochemical approach does not clarify whether the glycoconjugate of interest is a glycolipid or an *N*-glycosylated or *O*-glycosylated glycoprotein.

Reverse Proteomics/Genomics of the Galα1–3Gal Epitope—The unique expression profile of Galα1–3Gal in mouse epidermis prompted us to identify proteins that carry the Galα1–3Gal epitope in murine epidermis. Because all the observed glycans having the Galα1–3Gal epitope were biantennary oligosaccharides, we used ConA as an affinity reagent for the enrichment of the glycopeptides of interest. Immobilized

TABLE I

Observed signals of oligosaccharides released from murine skin glycoprotiens

Oligosaccharides indicated with an asterisk were detected also by a two-dimensional (2D) mapping technique. Structures were detemined by a two-dimensional mapping technique combined with sequential exoglycosidase digestions. Green square, GlcNAc; light blue square, GalNac; yellow circle, Man; dark blue circle, Gal; red inverted triangle; Hex, hexose; HexNac, *N*-acetylhexosamine; dHex, deoxyhexose.

No.	Observed (m/z)	compositon	epidermis Relative abundance (%) mean ± S.D. (n=3)	2D structures	dermis Relative abundance (%) mean ± S.D. (n=3)	2D structures
1	1016.4424	(Hex)1 (HexNAc)2	0.1 ± 0.1		0.2 ± 0.2	
2	1178.4952	(Hex)2 (HexNAc)2	6.6 ± 1.5		1.1 ± 0.6	
3	1324.5531	(Hex)2 (HexNAc)2 (Deoxyhexose)1	2.7 ± 0.5		1.4 ± 0.6	
4	1340.548	(Hex)3 (HexNAc)2	11.2 ± 0.8		1.3 ± 0.7	
5	1381.5746	(Hex)2 (HexNAc)3	0.3 ± 0.1		0.0 ± 0.0	
6	1486.6059	(Hex)3 (HexNAc)2 (Deoxyhexose)1	5.5 ± 2.0 *		0.6 ± 0.2	
7	1502.6008	(Hex)4 (HexNAc)2	4.0 ± 0.8 *		0.9 ± 0.2 *	
8	1543.6274	(HexNAc)1 + (Man)3(GlcNAc)2	1.3 ± 0.1 *		0.4 ± 0.1	
9	1648.6587	(Hex)4 (HexNAc)2 (Deoxyhexose)1	0.3 ± 0.1		0.0 ± 0.0	
10	1664.6536	(Hex)2 + (Man)3(GlcNAc)2	17.0 ± 1.6 *		9.0 ± 1.6 *	
11	1689.6853	(HexNAc)1 (Deoxyhexose)1 + (Man)3(GlcNAc)2	0.5 ± 0.1 *		0.8 ± 0.2	
12	1705.6802	(Hex)1 (HexNAc)1 + (Man)3(GlcNAc)2	1.9 ± 0.6 *		0.7 ± 0.1 *	
13	1746.7068	(HexNAc)2 + (Man)3(GlcNAc)2	1.1 ± 0.1		0.3 ± 0.1	
14	1810.7115	(Hex)2 (Deoxyhexose)1 + (Man)3(GlcNAc)2	0.1 ± 0.1		0.0 ± 0.0	
15	1826.7064	(Hex)3 + (Man)3(GlcNAc)2	9.5 ± 1.1 *		5.0 ± 0.4 *	
16	1848.7384	(HexNAc)1 (NeuAc)1 + (Man)3(GlcNAc)2	0.2 ± 0.2		0.1 ± 0.2	
17	1851.7381	(Hex)1 (HexNAc)1 (Deoxyhexose)1 + (Man)3(GlcNAc)2	1.7 ± 0.3 *		0.9 ± 0.3 *	
18	1867.733	(Hex)2 (HexNAc)1 + (Man)3(GlcNAc)2	0.7 ± 0.1		1.1 ± 0.2 *	
19	1892.7647	(HexNAc)2 (Deoxyhexose)1 + (Man)3(GlcNAc)2	0.5 ± 0.0 *		2.0 ± 0.6 *	
20	1908.7596	(Hex)1 (HexNAc)2 + (Man)3(GlcNAc)2	1.6 ± 0.1 *		0.5 ± 0.1 *	
21	1949.7862	(HexNAc)3 + (Man)3(GlcNAc)2	0.3 ± 0.0		0.0 ± 0.0	
22	1988.7592	(Hex)4 + (Man)3(GlcNAc)2	6.1 ± 0.6 *		2.2 ± 0.1 *	
23	1994.7963	(HexNAc)1 (Deoxyhexose)1 (NeuAc)1 + (Man)3(GlcNAc)2	0.1 ± 0.1		0.0 ± 0.0	
24	2010.7912	(Hex)1 (HexNAc)1 (NeuAc)1 + (Man)3(GlcNAc)2	0.1 ± 0.2		0.3 ± 0.0	
25	2013.7909	(Hex)2 (HexNAc)1 (Deoxyhexose)1 + (Man)3(GlcNAc)2	0.6 ± 0.2		0.5 ± 0.1	
26	2026.7912	(Hex)1 (HexNAc)1 (NeuGc)1 + (Man)3(GlcNAc)2	0.1 ± 0.1		0.5 ± 0.1	
27	2029.7858	(Hex)3 (HexNAc)1 + (Man)3(GlcNAc)2	0.4 ± 0.2 *		0.9 ± 0.0 *	
28	2054.8175	(Hex)1 (HexNAc)2 (Deoxyhexose)1 + (Man)3(GlcNAc)2	0.5 ± 0.1 *		1.7 ± 0.4 *	
29	2070.8124	(Hex)2 (HexNAc)2 + (Man)3(GlcNAc)2	1.9 ± 0.5 *		5.7 ± 0.5 *	
30	2095.8441	(HexNAc)3 (Deoxyhexose)1 + (Man)3(GlcNAc)2	0.1 ± 0.1		0.6 ± 0.1 *	
31	2111.839	(Hex)1 (HexNAc)3 + (Man)3(GlcNAc)2	0.5 ± 0.1		0.2 ± 0.2	
32	2150.812	(Hex)5 + (Man)3(GlcNAc)2	6.3 ± 0.3 *		2.4 ± 0.6 *	
33	2152.8656	(HexNAc)4 + (Man)3(GlcNAc)2	0.0 ± 0.0		0.0 ± 0.0	
34	2156.8491	(Hex)1 (HexNAc)1 (Deoxyhexose)1 (NeuAc)1 + (Man)3(GlcNAc)2	0.0 ± 0.0		0.0 ± 0.0	
35	2172.844	(Hex)2 (HexNAc)1 (NeuAc)1 + (Man)3(GlcNAc)2	0.2 ± 0.1		0.6 ± 0.1	
36	2175.8437	(Hex)3 (HexNAc)1 (Deoxyhexose)1 + (Man)3(GlcNAc)2	0.2 ± 0.0		0.0 ± 0.0	
37	2188.844	(Hex)2 (HexNAc)1 (NeuGc)1 + (Man)3(GlcNAc)2	0.1 ± 0.1		0.8 ± 0.1	
38	2191.8386	(Hex)4 (HexNAc)1 + (Man)3(GlcNAc)2	0.3 ± 0.0		0.0 ± 0.0	
39	2216.8703	(Hex)2 (HexNAc)2 (Deoxyhexose)1 + (Man)3(GlcNAc)2	2.8 ± 0.3 *		14.6 ± 1.5 *	
40	2232.8652	(Hex)3 (HexNAc)2 + (Man)3(GlcNAc)2	0.4 ± 0.1		0.0 ± 0.0	
41	2257.8969	(Hex)1 (HexNAc)3 (Deoxyhexose)1 + (Man)3(GlcNAc)2	0.5 ± 0.1		0.7 ± 0.1 *	
42	2273.8918	(Hex)2 (HexNAc)3 + (Man)3(GlcNAc)2	0.3 ± 0.1		0.0 ± 0.1	
43	2298.9235	(HexNAc)4 (Deoxyhexose)1 + (Man)3(GlcNAc)2	0.5 ± 0.0		0.0 ± 0.0	
44	2312.8648	(Hex)6 + (Man)3(GlcNAc)2	4.1 ± 0.7 *		1.7 ± 0.8 *	
45	2334.8968	(Hex)3 (HexNAc)1 (NeuAc)1 + (Man)3(GlcNAc)2	0.1 ± 0.2		0.4 ± 0.0	
46	2350.8968	(Hex)3 (HexNAc)1 (NeuGc)1 + (Man)3(GlcNAc)2	0.0 ± 0.0		0.5 ± 0.0	
47	2359.9285	(Hex)1 (HexNAc)2 (Deoxyhexose)1 (NeuAc)1 + (Man)3(GlcNAc)2 (HexNAc)2 (Deoxyhexose)2 (NeuGc)1 + (Man)3(GlcNAc)2	0.0 ± 0.0		0.3 ± 0.2	

TABLE I—*continued*

No.	Observed (m/z)	compositon	epidermis Relative abundance (%) mean ± S.D. (n=3)	2D structures	dermis Relative abundance (%) mean ± S.D. (n=3)	2D structures
48	2362.9282	(Hex)2 (HexNAc)2 (Deoxyhexose)2 + (Man)3(GlcNAc)2	1.3 ± 0.2		0.2 ± 0.2	
49	2375.9234	(Hex)2 (HexNAc)2 (NeuAc)1 + (Man)3(GlcNAc)2	0.0 ± 0.0		1.1 ± 0.2	
50	2378.9231	(Hex)3 (HexNAc)2 (Deoxyhexose)1 + (Man)3(GlcNAc)2	0.7 ± 0.1	•	0.7 ± 0.1	
51	2391.9234	(Hex)2 (HexNAc)2 (NeuGc)1 + (Man)3(GlcNAc)2	0.1 ± 0.1		5.2 ± 0.4	
52	2394.918	(Hex)4 (HexNAc)2 + (Man)3(GlcNAc)2	0.7 ± 0.1	•	0.0 ± 0.0	
53	2419.9497	(Hex)2 (HexNAc)3 (Deoxyhexose)1 + (Man)3(GlcNAc)2	0.4 ± 0.0		0.5 ± 0.1	
54	2435.9446	(Hex)3 (HexNAc)3 + (Man)3(GlcNAc)2	0.3 ± 0.1	•	0.0 ± 0.0	•
55	2476.9712	(Hex)2 (HexNAc)4 + (Man)3(GlcNAc)2	0.6 ± 0.1		0.0 ± 0.0	
56	2489.9915	(HexNAc)2 (Deoxyhexose)3 (NeuAc)1 + (Man)3(GlcNAc)2	0.0 ± 0.0		0.0 ± 0.0	
57	2505.9864	(Hex)1 (HexNAc)2 (Deoxyhexose)2 (NeuAc)1 + (Man)3(GlcNAc)2	0.0 ± 0.0		0.3 ± 0.3	
58	2508.9861	(Hex)2 (HexNAc)2 (Deoxyhexose)3 + (Man)3(GlcNAc)2	0.4 ± 0.0		0.0 ± 0.0	
59	2518.9816	(Hex)1 (HexNAc)2 (NeuAc)2 + (Man)3(GlcNAc)2	0.0 ± 0.0		0.2 ± 0.1	
60	2521.9813	(Hex)2 (HexNAc)2 (Deoxyhexose)1 (NeuAc)1 + (Man)3(GlcNAc)2	0.1 ± 0.1		1.1 ± 0.2	
61	2524.981	(Hex)3 (HexNAc)2 (Deoxyhexose)2 + (Man)3(GlcNAc)2	0.4 ± 0.0		0.0 ± 0.0	
62	2537.9813	(Hex)2 (HexNAc)2 (Deoxyhexose)1 (NeuGc)1 + (Man)3(GlcNAc)2	0.1 ± 0.1		15.3 ± 2.1	
63	2540.9759	(Hex)4 (HexNAc)2 (Deoxyhexose)1 + (Man)3(GlcNAc)2	1.2 ± 0.0	•	0.0 ± 0.0	
64	2553.9762	(Hex)3 (HexNAc)2 (NeuGc)1 + (Man)3(GlcNAc)2	0.1 ± 0.1		0.0 ± 0.0	
65	2560.0082	(HexNAc)3 (NeuAc)2 + (Man)3(GlcNAc)2	0.0 ± 0.0		0.2 ± 0.4	
66	2563.0079	(Hex)1 (HexNAc)3 (Deoxyhexose)1 (NeuAc)1 + (Man)3(GlcNAc)2	0.0 ± 0.0		0.0 ± 0.0	
67	2582.0025	(Hex)3 (HexNAc)3 (Deoxyhexose)1 + (Man)3(GlcNAc)2	0.2 ± 0.0		0.5 ± 0.5	•
68	2681.0344	(Hex)2 (HexNAc)2 (NeuAc)2 + (Man)3(GlcNAc)2	0.0 ± 0.0		0.1 ± 0.3	
69	2684.0341	(Hex)3 (HexNAc)2 (Deoxyhexose)1 (NeuAc)1 + (Man)3(GlcNAc)2 (Hex)2 (HexNAc)2 (Deoxyhexose)2 (NeuGc)1 + (Man)3(GlcNAc)2	0.1 ± 0.1		0.4 ± 0.1	
70	2713.0344	(Hex)2 (HexNAc)2 (NeuGc)2 + (Man)3(GlcNAc)2	0.1 ± 0.1		6.1 ± 1.7	
71	2725.0607	(Hex)2 (HexNAc)3 (Deoxyhexose)1 (NeuAc)1 + (Man)3(GlcNAc)2	0.0 ± 0.0		0.0 ± 0.0	
72	2741.0556	(Hex)3 (HexNAc)3 (NeuAc)1 + (Man)3(GlcNAc)2 (Hex)2 (HexNAc)3 (Deoxyhexose)1 (NeuGc)1 + (Man)3(GlcNAc)2	0.0 ± 0.0		0.2 ± 0.3	
73	2827.0923	(Hex)2 (HexNAc)2 (Deoxyhexose)1 (NeuAc)2 + (Man)3(GlcNAc)2	0.0 ± 0.0		0.5 ± 0.5	
74	2843.0923	(Hex)2 (HexNAc)2 (Deoxyhexose)1 (NeuAc)1 (NeuGc)1+ (Man)3(GlcNAc)2	0.0 ± 0.0		0.7 ± 0.2	
75	2859.0923	(Hex)2 (HexNAc)2 (Deoxyhexose)1 (NeuGc)2 + (Man)3(GlcNAc)2	0.0 ± 0.0		4.9 ± 1.6	
76	2887.1135	(Hex)3 (HexNAc)3 (Deoxyhexose)1 (NeuAc)1 + (Man)3(GlcNAc)2	0.0 ± 0.0		0.0 ± 0.0	
77	2900.1138	(Hex)2 (HexNAc)3 (NeuAc)1 (NeuGc)1 + (Man)3(GlcNAc)2 (Hex)1 (HexNAc)3 (Deoxyhexose)1 (NeuGc)2 + (Man)3(GlcNAc)2	0.0 ± 0.0		0.1 ± 0.2	
78	2903.1084	(Hex)4 (HexNAc)3 (NeuAc)1 + (Man)3(GlcNAc)2 (Hex)3 (HexNAc)3 (Deoxyhexose)1 (NeuGc)1 + (Man)3(GlcNAc)2	0.0 ± 0.0		0.4 ± 0.6	
79	3034.1454	(Hex)2 (HexNAc)2 (NeuGc)3 + (Man)3(GlcNAc)2	0.0 ± 0.0		0.4 ± 0.4	
80	3049.1663	(Hex)3 (HexNAc)3 (Deoxyhexose)2 (NeuGc)1 + (Man)3(GlcNAc)2 (Hex)4 (HexNAc)3 (Deoxyhexose)1 (NeuAc)1 + (Man)3(GlcNAc)2	0.0 ± 0.0		0.1 ± 0.1	
81	3192.2296	(Hex)3 (HexNAc)3 (Deoxyhexose)1 (NeuAc)2 + (Man)3(GlcNAc)2	0.0 ± 0.0		0.0 ± 0.0	
82	3369.2884	(Hex)5 (HexNAc)6 + (Man)3(GlcNAc)2	0.1 ± 0.2		0.0 ± 0.0	

ConA columns bind weakly to biantennary complex-type *N*-glycans, which can be eluted with 10 mM α-methylglucoside (20). Peptides were identified by off-line LC-MALDI-TOF/TOF analysis by analyzing the glycopeptide or by analyzing the peptide following PNGase F digestion.

We identified six glycoproteins with seven *N*-glycosylation sites that carry the Galα1–3Gal epitope (supplemental Fig. 1; summarized in Table II). Although we only identified a limited number of glycoproteins, they are likely to represent the major Galα1–3Gal proteins because we identified those glycopeptides with the strongest signal intensities. Among the six glycoproteins identified as carrying Galα1–3Gal, both desmoglein 1 and desmocollin 1 are components of intercellular desmosome junctions and are involved in the interaction of plaque proteins and intermediate filaments mediating cell-cell interactions (21). Integrin β4 is a glycoprotein that associates with the α6 integrin to form the α6-β4 complex, which functions as a receptor for laminin. Integrin β4 also plays a critical structural role in the hemidesmosome of epithelial cells (22). H2-K1 and H2-D1 are components of MHC class I (MHC-I),

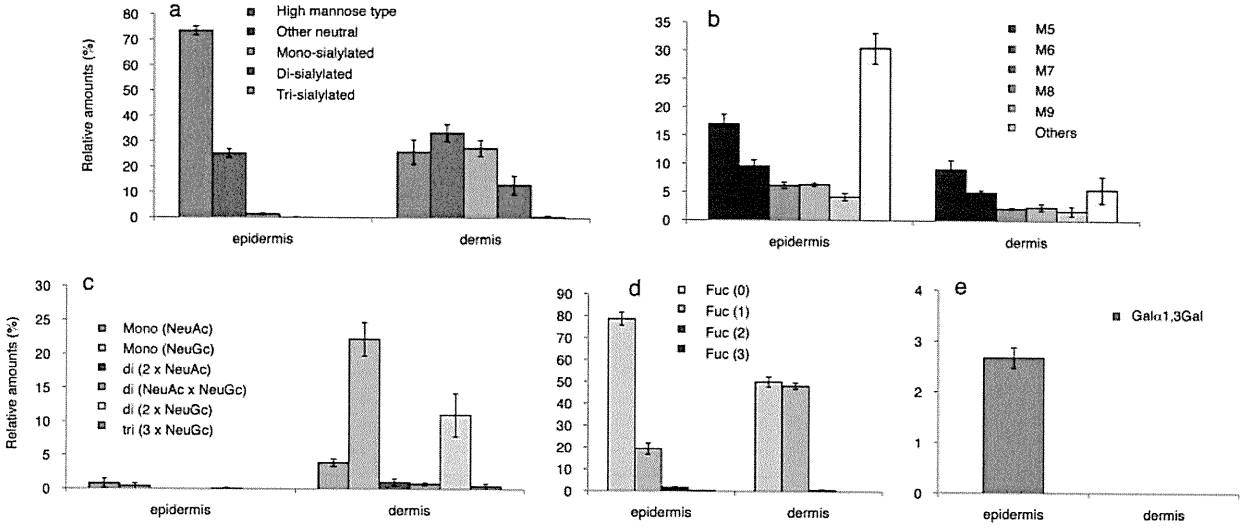

FIG. 2. **Summary of intertissue comparisons of the murine skin *N*-glycome.** *N*-Glycans quantified in each sample were classified according to the number of sialic acid residues in which neutral glycans were further categorized into high mannose-type glycans and others (*a*), the number of mannose residue(s) of high mannose-type glycans (*b*), forms and number of sialic acid residue(s) (*c*), the number of fucose residue(s) (*d*), and the presence of a Galα1–3Gal epitope (*e*). Values are shown as mean ± S.D. ($n = 3$). The classification was performed based on the estimated structures and compositions shown in Table I. Although six of the observed signals in Table I have two possible candidate compositions, they are all low abundance species, and identifying which of the two compositions is present is of negligible importance.

TABLE II

Summary of glycoprotiens identified as Galα1-3Gal epitope carriers

Glycosylation sites are underlined. ND, not detected.

Localization and protein name (gene name)	Swiss-Prot/TrEMBL Accession No.	Sequence	MASCOT Score	MASCOT Expect	Relative abundance (mean ± S.D.)					
					No. 29	No. 40	No. 52	No. 39	No. 50	No. 63
Desmosome										
Desmoglein *(Dsg1a or 1b or 1c)*	Q61495 or Q7TSF1 or Q7TSF0	LNATDADEPNNLNSMIAFK	43	0.0096	ND	ND	ND	ND	33.69 ± 17.75	66.31 ± 17.75
Desmocollin 1 *(Dsc1)*	P55849	NNQYNISVVATDTAGR	78	3.20E-06	67.40 ± 4.72	19.97 ± 3.01	12.63 ± 1.73	ND	ND	ND
Hemidesmosome										
Integrin β4 *(Itgb4)*	A2A863	TCNCSTGSLSDTQPCLR	53	0.00087	ND	ND	ND	ND	16.28 ± 11.24	83.72 ± 11.24
		SCDCPLSNATCIDSNGGICNGR	100	1.70E-08	ND	ND	ND	ND	ND	100.0 ± 0.0
MHC molecule										
H2-K1 protein *(H2-K1)*	P03991	YYNQSAGGSHTIQR	67	5.80E-05	ND	ND	ND	13.78 ± 2.36	10.66 ± 2.97	75.56 ± 5.28
H2-D1 protein *(H2-Q2)*	Q8R3Y0	TLLGYYNQSAGGTHTIQR	37	0.035	ND	ND	ND	ND	ND	100.0 ± 0.0
Unknown										
Sushi domain-containing protein 2 *(Susd2)*	Q9DBX3	FCILDVMSTGSSSVGNATR	45	0.0062	34.59 ± 2.68	16.02 ± 0.88	9.66 ± 1.77	12.61 ± 1.53	5.13 ± 1.10	21.99 ± 2.16

which noncovalently associates with β_2-microglobulin (23). MHC-I molecules display peptides from the intracellular pool at the cell surface for recognition by T lymphocytes bearing $\alpha\beta$ T cell receptor and mediate cell-cell adhesion by directly binding to CD8 (24–26). The functional role of sushi domain-containing protein-2 (Susd 2) is not known, but it contains the AMOP (adhesion associated domain in MUC4 and other proteins) domain, an ~100-residue extracellular domain that occurs in putative cell adhesion molecules and in some splice variants of MUC4; because this domain is found in extracellular domains involved in cell adhesion (27), it could be indicative of an adhesive role for this protein. All six glycoproteins commonly localize in extracellular space and are all *bona fide* or predicted type I transmembrane proteins.

We further determined the relative abundance of different microheterogeneous glycoforms present at a particular *N*-glycan binding site according to a method described previously (5) (Table II). Most glycoproteins identified as Galα1–3Gal epitope carriers were almost exclusively modified with oligosaccharides having the Galα1–3Gal epitope when the fraction weakly bound to an immobilized ConA column was used for the analysis. An exception was a glycopeptide of desmocollin 1 in which oligosaccharides with the Galα1–3Gal epitope were not the major glycoforms. We previously identified the same peptide to be glycosylated with high mannose-type oligosaccharides when a fraction strongly bound to an immobilized ConA column was used for the analysis (5). To clarify the relative quantities of the micro-

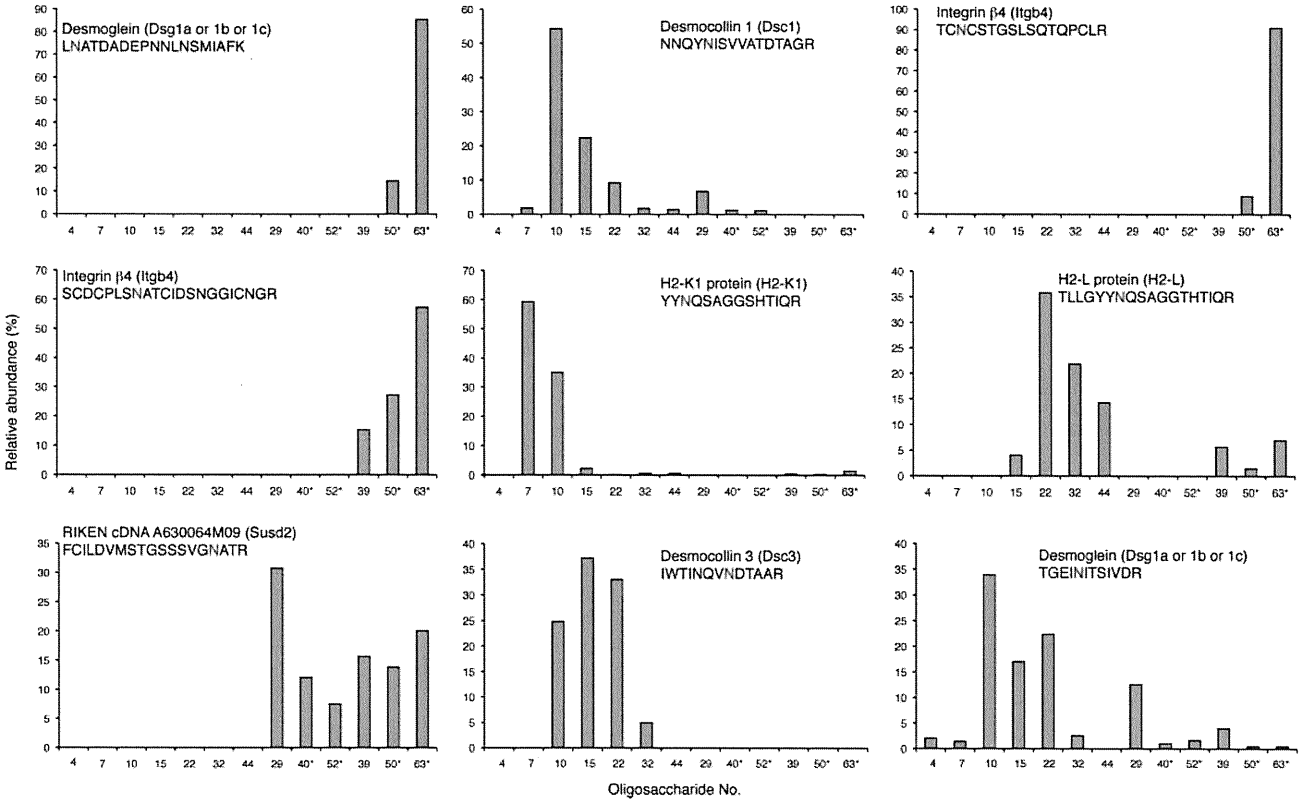

FIG. 3. **Microheterogeneity of glycoforms present at each *N*-glycosylation site of seven glycopeptides identified as carrying a Galα1–3Gal epitope.** Two glycopeptides identified previously as carrying high mannose-type oligosaccharides were also analyzed for their microheterogeneity. The *numbers* correspond to the structures in Table I. An *asterisk* indicates that the oligosaccharide possesses a Galα1–3Gal epitope.

heterogeneous glycoforms present on the glycopeptides, fractions both weakly and strongly bound to the immobilized ConA column were collected in gross, and the relative quantities of the microheterogeneous glycoforms present at each *N*-glycan binding site were determined. In addition to seven glycopeptides identified as modified with the Galα1–3Gal epitope, we analyzed two glycopeptides determined previously to be modified with high mannose-type oligosaccharides (Fig. 3). This analysis revealed that the glycopeptide of interest from desmocollin 1 is dominantly modified with high mannose-type oligosaccharides, and the relative proportion of Galα1–3Gal was nominal. The same tendency was observed also for the peptides of the H2-K1 and H2-D1 proteins. The remaining glycopeptides were dominantly modified with oligosaccharides having the Galα1–3Gal epitope. This analysis also revealed that the microheterogeneity of the two different glycosylation sites (underlined) on desmoglein 1 are completely different; LNATDADEPNNLNSMIAFK is dominantly modified with oligosaccharides having the Galα1–3Gal epitope, whereas TGEINITSIVDR is dominantly modified with high mannose-type oligosaccharides. These observations indicate that the Galα1–3Gal epitope is preferentially attached to adhesion molecules, and the spatial arrangement of this epitope on the protein is highly regulated.

Mice deficient in α3GalT-1 develop cortical cataracts within 4–6 weeks of birth (28). Although no other notable pathological abnormality has been detected, these α3GalT-1-deficient animals retain a residual level of the αGal epitope possibly because of compensation by α3GalT-2 (29, 30). Very recently, transgenic mice that systemically express endo-β-galactosidase C, which removes the terminal Galα1–3Gal disaccharide, were produced. Flow cytometry and histochemical analyses showed that the Galα1–3Gal epitope was completely removed from at least restricted organs including skin, heart, and lung. Of a total of six founder mice obtained, three were unable to survive after birth because they had severe phenotypes, including edema and dry skin that resulted in loss of moisture from the skin surface and finally to cracking of the skin in the neonatal stage (31). Despite the marked pathologic lesions in the epidermis, the dermis was normal in structure (32). These observations agree well with the distribution of the Galα1–3Gal epitope in the murine dermis and epidermis shown in the current study. Proteins identified as Galα1–3Gal carriers in this study may contribute to the severe phenotypes seen upon failure of proper α-galactosylation.

To further validate these findings, we compared our proteome data with the tissue distributions derived from the enormous amount of expression data present in the SymAtlas

of the Genomics Institute of the Novartis Research Foundation (33). Among the six proteins identified, desmoglein 1, desmocollin 1, and integrin β4 are highly selectively expressed in epidermis, digits, and tongue. H2-K1 and H2-D1 are most highly expressed in B cells and T cells but are also expressed in various other tissues and organs including lymph node, trachea, adipose tissue, epidermis, lung, spleen, and small intestines. Susd 2 is ubiquitously expressed, but it is expressed most highly in umbilical cord and dorsal root ganglia followed by epidermis, trigeminal, and kidney. The transcriptional profiling data of *α3GalT-1* shows that it is ubiquitously expressed but is most highly expressed in the female reproductive system (*e.g.* in fertilized egg, oocyte, blastocytes, and placenta)(supplemental Fig. 2) consistent with previous findings that the terminal Galα1–3Gal epitope is crucial for murine sperm-egg binding (34) and recognition during initial gamete binding (35). The expression levels of *Ggta1* in epidermis and eye are either slightly higher or equal to the median, thus making it very difficult to predict the phenotypes detected in α3GalT-1-deficient mice and transgenic mice expressing endo-β-galactosidase C by transcriptomics data alone. We could discover that the Galα1–3Gal epitope specifically modifies adhesion molecules, which can possibly explain the phenotypes seen in transgenic mice, by using the approach to link the glycome to the proteome and transcriptome. The transcriptomics data indicate that desmoglein 1 and integrin β4 are also moderately expressed in the eye; therefore, these molecules may be involved in the incidence of cortical cataracts seen in α3GalT-1-deficient mice.

Identification of Galα1–3Gal Epitope-recognizing Molecule in Murine Epidermis—*N*-Glycosylation has been shown to modulate the adhesion properties of proteins, such as the association of the α5 and β1 subunits of integrin, and receptor functioning (36, 37). In this regard, the adhesion molecule-specific glycosylation by the Galα1–3Gal epitope in murine epidermis may also be involved in the modulation of the adhesion properties of proteins. As a trial to explore this possibility, genes of which epidermal expression is more than 10-fold over median expression levels were searched on SymAtlas. Among the list, six genes are Gene Ontology-annotated as "sugar binding." They are *Aim1*, *Lgals3*, *Lgals7*, *Mgl1*, *Mgl2*, and *Mrc1*, each encoding absent in melanoma 1, galectin-3, galectin-7, macrophage galactose *N*-acetylgalactosamine-specific lectin 1, macrophage galactose *N*-acetylgalactosamine-specific lectin 2, and macrophage mannose receptor 1, respectively.

Galectins are a group of relatively small lectins whose ability to bind to β-galactosides is evolutionarily conserved among extensive organisms. Galectin-3 is expressed and secreted by various types of cells, especially monocytes, macrophages, mast cells, and epithelial cells including corneal epithelium (38). It is a mitogen capable of stimulating fibroblast cell proliferation in a paracrine fashion through interaction with cell surface glycoconjugates (39). This protein can also exert an antiapoptotic activity underscoring its strong effect on cell growth (40). Unlike galectin-3, expression of galectin-7 is restricted to epithelia that are stratified or are destined to become stratified (41). Galectin-7 is thought to play a role in apoptosis (42). The carbohydrate binding specificities of galectins have been elucidated by many researchers. Notably Hirabayashi *et al.* (43) extensively analyzed the interaction of galectins, including galectin-3 and -7, by frontal affinity chromatography using 41 glycans (including 12 *N*-glycans). To our knowledge, however, the interaction of galectin-3 and -7 with *N*-glycans having the Galα1–3Gal epitope(s) has not been elucidated. Therefore, we examined the interaction of galectin-3 and -7 with various naturally derived *N*-glycans including the biantennary oligosaccharide having two Galα1–3Gal epitopes at the non-reducing termini (number 63 in Table I) by SPR. Following the biotinylation of each oligosaccharide, they were immobilized onto the streptavidin preimmobilized surfaces. The molar amount of each immobilized oligosaccharide is presumed to be nearly constant because the amount of streptavidin was constant, and an excess of purified biotinylated oligosaccharide was introduced (16). The validity of the immobilization of each *N*-glycan was quantitatively confirmed by measuring interactions with ConA and RCA_{120}, whose sugar binding specificities are well characterized (supplemental Fig. 3).

The murine galectin-3 and -7 were passed over the sensor surface at concentrations of 0.7 and 1.3 μM, respectively, and binding was monitored as changes in the SPR signal. As shown in Fig. 4*a*, the bindings of galectin-3 differed markedly depending on the structure of the immobilized *N*-glycans. *N*-Glycans having two Galα1–3Gal epitopes gave the highest increase in the resonance signal followed by an *N*-glycan with one Galα1–3Gal epitope. *N*-Glycans terminated with Galβ1–4GlcNAc also interacted with galectin-3, but the response was much lower. These results indicate that galectin-3 has higher affinity to Galα1–3Galβ1–4GlcNAc epitope than to Galβ1–4GlcNAc. Interestingly we observed that the presence or absence of core fucose on the *N*-glycan with two Galα1–3Gal epitopes affects the interaction with galectin-3; the presence of core fucose further increased the binding of galectin-3. This may be attributable to the conformational change of *N*-glycan. The presence of core fucose has been reported to have a dramatic effect on the conformation of the Manα1–6 antenna resulting in the reduced flexibility of this antenna (44). Note that *N*-glycosylation sites of desmoglein-1 and integrin β4 identified to have Galα1–3Gal epitopes are almost solely occupied by the *N*-glycan having two Galα1–3Gal epitopes and core fucose. On the contrary, the increase in resonance signal upon injection of galectin-7 was marginal (Fig. 4*b*).

Although similar gene expression patterns do not necessarily mean that these two gene pairs are related, our analysis clearly demonstrated that galectin-3 preferentially binds to *N*-glycan with the Galα1–3Gal epitope than those without this epitope and thus strongly suggested that the extracellular

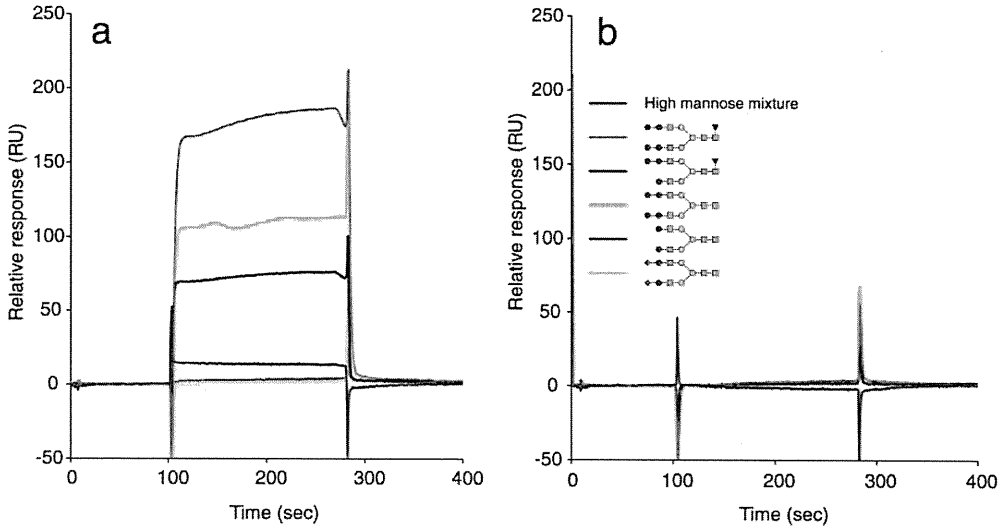

FIG. 4. **Sensorgrams showing the interaction of immobilized oligosaccharides with galectins.** *a*, murine galectin-3; *b*, murine galectin-7.

portion of cell surface adhesion proteins (*e.g.* desmoglein and integrin) would associate with galectin-3 via Galα1–3Gal epitopes on their *N*-glycans at epidermis. The biological significance of the interaction of galectin-3 with cell surface adhesion proteins needs to be further elucidated. Galectin-3 may mediate cell-cell/cell-extracellular matrix interactions or act as deadhesion molecule as shown in the interaction of thymocytes and thymic microenvironmental cells (45).

Glycomics of Human Dermis and Epidermis—The Galα1–3Gal structure is abundantly expressed in glycoproteins and glycolipids of nonprimate mammals and New World monkeys but is not present in Old World monkeys, apes, and humans (46–48). Therefore, we turned our focus to human epidermal glycomics and glycoproteomics. To our knowledge, the glycomics of the human dermis and epidermis have not been studied extensively.

We quantitatively analyzed human dermal and epidermal glycome using the same procedure described for the murine glycomics; the MALDI-TOF spectra are shown in supplemental Fig. 4. We estimated the structure and relative abundance of each signal (supplemental Table 1), and we analyzed the relative abundance of each type of structure in the oligosaccharides observed in each sample (Fig. 5). The glycomic profiles of both the epidermis and dermis were fairly similar between mouse and human. The high mannose-type oligosaccharides (including M2, M3, and M4 and their fucosylated analogues) were relatively abundant (Fig. 5, *a* and *b*), and the sialylated and fucosylated species were of relatively low abundance in human epidermis (Fig. 5, *c* and *d*) as they were for mice. The interspecies differences in dermal glycomic profiles were mostly limited to the extent and form of sialylation: human contains only NeuAc, whereas mouse contains both NeuAc and NeuGc. As a result, the signals observed in the higher molecular mass region of the dermal glycome spectra often shifted by 16 or 32 Da increments between human and mouse.

As expected, no glycans carrying the Galα1–3Gal epitope were observed in human dermis or epidermis. Instead we found that the expression of oligosaccharides with the GalNAcβ1–4GlcNAc (*N,N'*-diacetyllactosediamine; LacdiNAc) epitope was exceptionally high in the human epidermis (Fig. 5*e*). The presence of the LacdiNAc epitope were confirmed based on two-dimensional LC mapping as well as the MDSF method in MALDI-TOF/TOF mass spectrometry as exemplified in supplemental Fig. 5. The LacdiNAc epitope is common on the glycoproteins of invertebrates, such as helminth parasites, but is also found on some mammalian glycoproteins (49). In vertebrates, the group of glycoproteins that carries the LacdiNAc epitope is diverse and includes membrane as well as secreted glycoproteins, enzymes, hormones, transport proteins, and protective glycoproteins (50, 51).

It is not clear at this point whether the LacdiNAc epitope plays an important role in human epidermis as the Galα1–3Gal epitope does in murine epidermis. However, it is noteworthy that it was reported that a remarkably strict co-localization of galectin-3-reactive binding sites with desmoglein was found by immunohistochemical analysis of human corneal and conjunctival epithelia (52). Although no detailed mechanism underlying the interaction of galectin-3 and desmosomal proteins has been elucidated to date, the LacdiNAc epitope may mediate the interaction of these molecules. It may be interesting to note also that the conjunctive epithelium from the patient with Stevens-Johnson syndrome, a serious and potentially life-threatening cutaneous drug reaction, expressed no galectin-3-reactive binding sites (52). Future glycomics and glycoproteomics analyses of various skin disorders would enable the significance of the presence of the LacdiNAc epitope in epidermis to be elucidated.

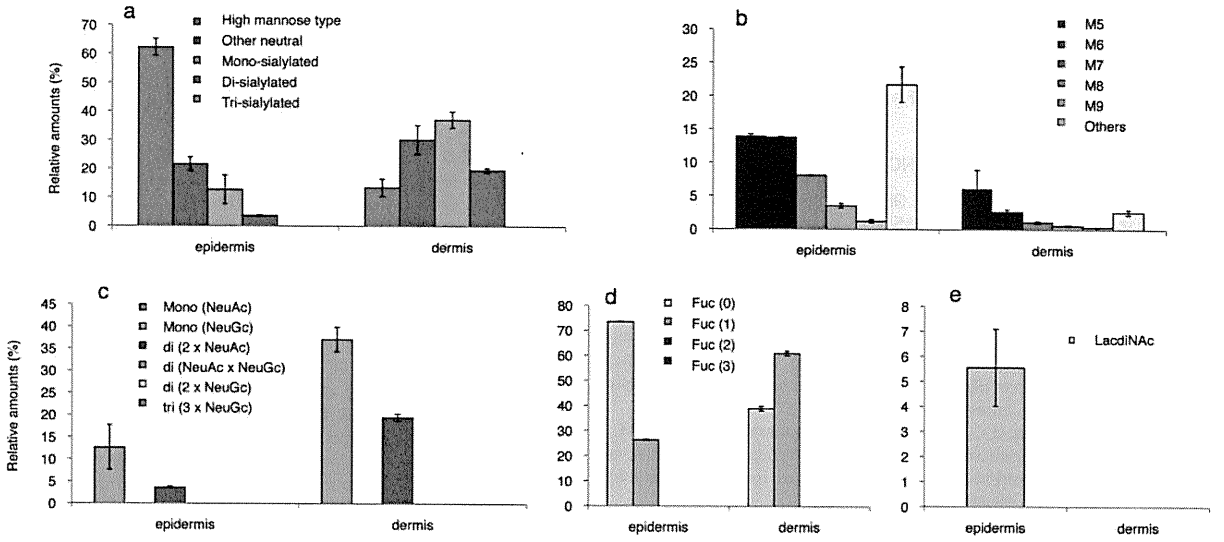

FIG. 5. **Summary of intertissue comparisons of human skin *N*-glycome.** *N*-Glycans quantified in each sample were classified according to the number of sialic acid residues in which neutral glycans were further categorized into high mannose-type glycans and others (*a*), the number of mannose residue(s) of high mannose-type glycans (*b*), forms and number of sialic acid residue(s) (*c*), the number of fucose residue(s) (*d*), and the presence of the LacdiNAc epitope (*e*). The classification was performed based on the estimated structure and composition shown in supplemental Table 1. Although six of the observed signals in supplemental Table 1 have two possible candidate compositions, they are all species of low abundance, and identifying which of the two compositions is present is of negligible importance.

Conclusion—In this study, we evaluated the murine skin glycomics and glycoproteomics in detail, including sialylated species, based on a recently established glycoblotting technique and MALDI-TOF/TOF MS analysis. One of the key findings was that the Galα1–3Gal epitope is highly selectively attached to adhesion molecules of murine epidermis in a glycosylation site-specific manner. These findings provide mechanistic insight into the causal connection between the genotype and the phenotype seen in α3GalT-1-deficient mice and transgenic mice expressing endo-β-galactosidase C. Because protein glycosylation is very complicated, it is not possible with the current methodology to fully characterize the *N*-glycosylation of proteins on a proteome-wide scale in terms of the glycosylation site, oligosaccharide structure, and quantitative microheterogeneity. Very complex forms of transcriptional and post-translational modifications can, in principle, be analyzed with state-of-the-art top-down MS methods if sufficient amounts of a purified protein are available (53); however, major technological breakthroughs are needed to achieve the purification of the protein(s) of interest and high throughput protein analysis.

The correlation function of the searchable SymAtlas database was then used to refine genes with an expression similar to proteins identified to carry Galα1–3Gal epitope. Molecular interaction analysis using naturally derived *N*-glycans with or without the Galα1–3Gal epitope experimentally demonstrated that *N*-glycan with not only Galα1–3Gal epitope but also the core fucose is a preferred glycan ligand for galectin-3. Finally comparative glycomics of murine and human epidermis indicated that the LacdiNAc epitope, rather than the Galα1–3Gal epitope, was highly expressed in human epidermis, although its functions remain to be elucidated.

Glycoform-focused reverse genomics is a novel approach that links data from different omics by first obtaining exhaustive quantitative glycomics data and then tracing from the glycome back to the proteome and transcriptome. This reverse approach allows novel classification of proteins and genes with regard to the significance of glycosylation in a way that is not possible with the information that can currently be obtained from genomic, transcriptomic, and traditional proteomic information alone. This concept would find wide application for the identification of diagnostic biomarkers and therapeutic targets.

Acknowledgment—We thank Prof. S.-i. Hakomori for critical reading of the manuscript and valuable comments.

* This work was supported by Special Coordination Funds for Promoting Science and Technology of the Ministry of Education, Culture, Sports, Science, and Technology, the Japanese Government and by Grant-in-aid for Scientific Research 18550145 from the Ministry of Education, Science, Sports, and Culture of Japan. The costs of publication of this article were defrayed in part by the payment of page charges. This article must therefore be hereby marked "*advertisement*" in accordance with 18 U.S.C. Section 1734 solely to indicate this fact.

[S] The on-line version of this article (available at http://www.mcponline.org) contains supplemental material.

§ To whom correspondence may be addressed: Graduate School of Advanced Life Science, Frontier Research Center for Post-Genomic Science and Technology, Hokkaido University, Sapporo 001-0021, Japan. Tel.: 81-11-706-9043; Fax: 81-11-706-9042; E-mail: yshinohara@glyco.sci.hokudai.ac.jp.

‖ To whom correspondence may be addressed: Graduate School of Advanced Life Science, Frontier Research Center for Post-Genomic Science and Technology, Hokkaido University, Sapporo 001-0021, Japan. Tel.: 81-11-706-9043; Fax: 81-11-706-9042; E-mail: shin@glyco.sci.hokudai.ac.jp.

REFERENCES

1. Ohtsubo, K., and Marth, J. D. (2006) Glycosylation in cellular mechanisms of health and disease. *Cell* **126,** 855–867
2. Madison, K. C. (2003) Barrier function of the skin: "la raison d'être" of the epidermis. *J. Investig. Dermatol.* **121,** 231–241
3. Mehul, B., Corre, C., Capon, C., Bernard, D., and Schmidt, R. (2003) Carbohydrate expression and modification during keratinocyte differentiation in normal human and reconstructed epidermis. *Exp. Dermatol.* **12,** 537–545
4. Dabelsteen, E., Buschard, K., Hakomori, S.-i., and Young, W. W. (1984) Pattern of distribution of blood group antigens on human epidermal cells during maturation. *J. Investig. Dermatol.* **82,** 13–17
5. Uematsu, R., Furukawa, J.-i., Nakagawa, H., Shinohara, Y., Deguchi, K., Monde, K., and Nishimura, S.-I. (2005) High throughput quantitative glycomics and glycoform-focused proteomics of murine dermis and epidermis. *Mol. Cell. Proteomics* **4,** 1977–1989
6. Nishimura, S.-I., Niikura, K., Kurogochi, M., Matsushita, T., Fumoto, M., Hinou, H., Kamitani, R., Nakagawa, H., Deguchi, K., Miura, N., Monde, K., and Kondo, H. (2005) High-throughput protein glycomics: combined use of chemoselective glycoblotting and MALDI-TOF/TOF mass spectrometry. *Angew. Chem. Int. Ed. Engl.* **44,** 91–96
7. Furukawa, J.-i., Shinohara, Y., Kuramoto, H., Miura, Y., Shimaoka, H., Kurogochi, M., Nakano, M., and Nishimura, S.-I. (2008) A comprehensive approach to structural and functional glycomics based on chemoselective glycoblotting and sequential tag conversion. *Anal. Chem.,* **80,** 1094–1101
8. Miura, Y., Hato, M., Shinohara, Y., Kuramoto, H., Furukawa, J.-i., Kurogochi, M., Shimaoka, H., Tada, M., Nakanishi, K., Ozaki, M., Todo, S., and Nishimura, S.-I. (2008) BlotGlycoABC™, an integrated glycoblotting technique for rapid and large scale clinical glycomics. *Mol. Cell. Proteomics* **7,** 370–377
9. Bligh, E. G., and Dyer, W. J. (1959) A rapid method of total lipid extraction and purification. *Can. J. Biochem. Physiol.* **37,** 911–917
10. Kita, Y., Miura, Y., Furukawa, J-i., Nakano, M., Shinohara, Y., Ohno, M., Takimoto, A., and Nishimura S.-I. (2007) Quantitative glycomics of human whole serum glycoproteins based on the standardized protocol for liberating *N*-glycans. *Mol. Cell. Proteomics* **6,** 1437–1445
11. Nakagawa, H., Kawamura, Y., Kato, K., Shimada, I., Arata, Y., and Takahashi, N. (1995) Identification of neutral and sialyl *N*-linked oligosaccharide structures from human serum glycoproteins using three kinds of high-performance liquid chromatography. *Anal. Biochem.* **226,** 130–138
12. Takahashi, N., Nakagawa, H., Fujikawa, K., Kawamura, Y., and Tomiya, N. (1995) Three-dimensional elution mapping of pyridylaminated *N*-linked neutral and sialyl oligosaccharides. *Anal. Biochem.* **226,** 139–146
13. Kurogochi, M., and Nishimura, S.-I. (2004) Structural characterization of *N*-glycopeptides by matrix-dependent selective fragmentation of MALDI-TOF/TOF tandem mass spectrometry. *Anal. Chem.* **76,** 6097–6101.
14. Hato, M., Nakagawa, H., Kurogochi, M., Akama, T. O., Marth, J. D., Fukuda, M. N., and Nishimura, S. (2006) Unusual *N*-glycan structures in alpha-mannosidase II/IIx double null embryos identified by a systematic glycomics approach based on two-dimensional LC mapping and matrix-dependent selective fragmentation method in MALDI-TOF/TOF mass spectrometry. *Mol. Cell. Proteomics* **5,** 2146–2157
15. Naka, R., Kamoda, S., Ishizuka, A., Kinoshita, M., and Kakehi, K. (2006) Analysis of total *N*-glycans in cell membrane fractions of cancer cells using a combination of serotonin affinity chromatography and normal phase chromatography. *J. Proteome Res.* **5,** 88–97
16. Shinohara, Y., Sota, H., Gotoh, M., Hasebe, M., Tosu, M., Nakao, J., Hasegawa, Y., and Shiga, M. (1996) Bifunctional labeling reagent for oligosaccharides to incorporate both chromophore and biotin groups. *Anal. Chem.* **68,** 2573–2579
17. Dennis, J. W., Granovsky, M., and Warren, C. E. (1999) Protein glycosylation in development and disease. *BioEssays* **21,** 412–421
18. Walsh, A., and Chapman, S. J. (1991) Sugars protect desmosome and corneosome glycoproteins from proteolysis". *Arch. Dermatol. Res.* **283,** 174–179
19. Nemanick, M. K., Whitehead, S. J., and Elias, P. M. (1983) Alternations in membrane sugars during epidermal differentiation: visualization with lectins and role of glycosidases. *J. Histochem. Cytochem.* **38,** 887–897
20. Ogata, S., Muramatsu, T., and Kobata, A. (1975) Fractionation of glycopeptides by affinity column chromatography on concanavalin A-Sepharose. *J. Biochem.* **78,** 687–696
21. Kottke, M. D., Delva, E., and Kowalczyk, A. P. (2006) The desmosome: cell science lessons from human diseases. *J. Cell Sci.* **119,** 797–806
22. Gil, S. G., Brown, T. A., Ryan, M. C., and Carter, W. G. (1994) Junctional epidermolysis bullosis: defects in expression of epiligrin/nicein/kalinin and integrin β4 that inhibit hemidesmosome formation. *J. Investig. Dermatol.* **103,** 31S–38S
23. Rosenthal, A., Wright, S., Cedar, H., Flavell, R., and Grosveld, F. (1984) Regulated expression of an introduced MHC H-2K bm1 gene in murine embryonal carcinoma cells. *Nature* **310,** 415–418
24. Norment, A. M., Salter, R. D., Parham, P., Engelhard, V. H., and Littman, D. R. (1988) Cell-cell adhesion mediated by CD8 and MHC class I molecules. *Nature* **336,** 79–81
25. Jelonek, M. T., Classon, B. J., Hudson, P. J., and Margulies, D. H. (1998) Direct binding of the MHC class I molecule H-2Ld to CD8: interaction with the amino terminus of a mature cell surface protein. *J. Immunol.* **160,** 2809–2814
26. Buus, S., Sette, A., Colon, S. N., Miles, C., and Grey, H. M. (1987) The relation between major histocompatibility complex (MHC) restriction and the capacity of Ia to bind immunogenic peptides. *Science* **235,** 1353–1358
27. Ciccarelli, F. D., Doerks, T., and Bork, P. (2002) AMOP, a protein module alternatively spliced in cancer cells. *Trends Biochem. Sci.* **27,** 113–115
28. Tearle, R. G., Tange, M. J., Zannettino, Z. L., Katerelos, M., Shinkel, T. A., Van Denderen, B. J., Lonie, A. J., Lyons, I., Nottle, M. B., Cox, T., Becker, C., Peura, A. M., Wigley, P. L., Crawford, R. J., Robins, A. J., Pearse, M. J., and d'Apice, A. J. (1996) α-1,3-Galactosyltransferase knockout mouse. Implications for xenotransplantation. *Transplantation* **61,** 13–19
29. Milland, J., Christiansen, D., Lazarus, B. D., Taylor, S. G., Xing, P. X., and Sandrin, M. S. (2006) The molecular basis for galα(1,3)gal expression in animals with a deletion of the α1,3 galactosyltransferase gene. *J. Immunol.* **176,** 2448–2454
30. Taylor, S. G., McKenzie, I. F., and Sandrin, M. S. (2003) Characterization of the rat α(1,3)galactosyltransferase: evidence for two independent genes encoding glycosyltransferases that synthesize Galα(1,3)Gal by two separate glycosylation pathways. *Glycobiology* **13,** 327–337
31. Watanabe, S., Misawa, M., Matsuzaki, T., Sakurai, T., Muramatsu, T., Yokomine, T. A., and Sato, M. (2008) Production and characterization of transgenic mice systemically expressing endo-β-galactosidase C. *Glycobiology* **18,** 9–19
32. Misawa, M., Watanabe, S., Ihara, S., Muramatsu, T., and Matsuzaki, T. (2008) Accelerated proliferation and abnormal differentiation of epidermal keratinocytes in endo-β-galactosidase C transgenic mice. *Glycobiology* **18,** 20–27
33. Su, A. I., Cooke, M. P., Ching, K. A., Hakak, Y., Walker, J. R., Wiltshire, T., Orth, A. P., Vega, R. G., Sapinoso, L. M., Moqrich, A., Patapoutian, A., Hampton, G. M., Schultz, P. G., and Hogenesch, J. B. (2002) Large-scale analysis of the human and mouse transcriptomes. *Proc. Natl. Acad. Sci. U. S. A.* **99,** 4465–4470
34. Bleil, J. D., and Wassarman, P. M. (1988) Galactose at the nonreducing terminus of O-linked oligosaccharides of mouse egg zona pellucida glycoprotein ZP3 is essential for the glycoprotein's sperm receptor activity. *Proc. Natl. Acad. Sci. U. S. A.* **85,** 6778–6782
35. Litscher, E. S., Juntunen, K., Seppo, A., Penttila, L., Niemela, R., Renkonen, O., and Wassarman, P. M. (1995) Oligosaccharide constructs with defined structures that inhibit binding of mouse sperm to unfertilized eggs in vitro. *Biochemistry* **34,** 4662–4669
36. Nadanaka, S., Sato, C., Kitajima, K., Katagiri, K., Irie, S., and Yamagata, T. (2001) Occurrence of oligosialic acids on integrin α5 subunit and their involvement in cell adhesion to fibronectin. *J. Biol. Chem.* **276,** 33657–33664
37. Zheng, M., Fang, H., and Hakomori, S.-i. (1994) Functional role of *N*-glycosylation in α5β1 integrin receptor. De-*N*-glycosylation induces dissociation or altered association of α5 and β1 subunits and concomitant loss of fibronectin binding activity. *J. Biol. Chem.* **269,** 12325–12331
38. Gupta, S. K., Masinick, S., Garrett, M., and Hazlett, L. D. (1997) Pseudomonas aeruginosa lipopolysaccharide binds galectin-3 and other human

corneal epithelial proteins. *Infect. Immun.* **65,** 2747–2753
39. Inohara, H., Akahani, S., and Raz. A. (1998) Galectin-3 stimulates cell proliferation. *Exp. Cell Res.* **245,** 294–302
40. Yang, R. Y., Hsu, D. K., and Liu, F. T. (1996) Expression of galectin-3 modulates T-cell growth and apoptosis. *Proc. Natl. Acad. Sci. U. S. A.* **93,** 6737–6742
41. Magnaldo, T., Fowlis, D., and Darmon, M. (1998) Galectin-7, a marker of all types of stratified epithelia. *Differentiation* **63,** 159–168
42. Bernerd, F., Sarasin, A., and Magnaldo, T. (1999) Galectin-7 overexpression is associated with the apoptotic process in UVB-induced sunburn keratinocytes. *Proc. Natl. Acad. Sci. U. S. A.* **96,** 11329–11334
43. Hirabayashi, J., Hashidate, T., Arata, Y., Nishi, N., Nakamura, T., Hirashima, M., Urashima, T., Oka, T., Futai, M., Muller, W. E., Yagi, F., and Kasai, K. (2002) Oligosaccharide specificity of galectins: a search by frontal affinity chromatography. *Biochim. Biophys. Acta* **1572,** 232–254
44. Stubbs, H. J., Lih, J. J., Gustafson, T. L., and Rice, K. G. (1996) Influence of core fucosylation on the flexibility of a biantennary *N*-linked oligosaccharide. *Biochemistry* **35,** 937–947
45. Villa-Verde, D. M., Silva-Monteiro, E., Jasiulionis, M. G., Farias-De-Oliveira, D. A., Brentani, R. R., Savino, W., and Chammas, R. (2002) Galectin-3 modulates carbohydrate-dependent thymocyte interactions with the thymic microenvironment. *Eur. J. Immunol.* **32,** 1434–1444
46. Eto, T., Iichikawa, Y., Nishimura, K., Ando, S., and Yamakawa, T. (1968) Chemistry of lipid of the posthemyolytic residue or stroma of erythrocytes. XVI. Occurrence of ceramide pentasaccharide in the membrane of erythrocytes and reticulocytes of rabbit. *J. Biochem.* **64,** 205–213
47. Stellner, K., Saito, H., and Hakomori, S.-i. (1973) Determination of aminosugar linkages in glycolipids by methylation. Aminosugar linkages of ceramide pentasaccharides of rabbit erythrocytes and of Forssman antigen. *Arch. Biochem. Biophys.* **155,** 464–472
48. Uri, G., and Tanemura, M. (1999) Significance of α-Gal (Galα1-3Galβ1–4GlcNAc-R) Epitopes and α1, 3 Galactosyltransferase in xenotransplantation. *Trends Glycosci. Glycotechnol.* **11,** 317–327
49. Cummings, R. D., and Nyame, A. K. (1999) Schistosome glysoconjugates. *Biochim. Biophys. Acta* **1455,** 363–374
50. Green, E. D., and Baenziger, J. U. (1988) Asparagine-linked oligosaccharides on lutropin, follitropin, and thyrotropin. II. Distributions of sulfated and sialylated oligosaccharides on bovine, ovine, and human pituitary glycoprotein hormones. *J. Biol. Chem.* **263,** 36–44
51. Hooper, L. V., Hindsgaul, O., and Baenziger, J. U. (1995) Purification and characterization of the GalNAc-4-sulfotransferase responsible for sulfation of GalNAc β 1,4GlcNAc-bearing oligosaccharides. *J. Biol. Chem.* **270,** 16327–16332
52. Hrdlicková-Cela, E., Plzák, J., Smetana, K. Jr., Mělková, Z., Kaltner, H., Filipec, M., Liu, F. T., and Gabius, H. J. (2001) Detection of galectin-3 in tear fluid at disease states and immunohistochemical and lectin histochemical analysis in human corneal and conjunctival epithelium. *Br. J. Ophthalmol.* **85,** 1336–1340
53. Godovac-Zimmermann, J., Mulvey, C., Konstantoulaki, M., Sainsbury, R., and Brown, L. R. (2007) Promise of multiphoton detection in discovery and diagnostic proteomics. *Expert Rev. Proteomics* **4,** 161–173

Development 136, 367-372 (2009) doi:10.1242/dev.021295

Embryonic hair follicle fate change by augmented β-catenin through Shh and Bmp signaling

Kentaro Suzuki[1,2], Yuji Yamaguchi[3], Mylah Villacorte[1,2], Kenichiro Mihara[1], Masashi Akiyama[4], Hiroshi Shimizu[4], Makoto M. Taketo[5], Naomi Nakagata[1], Tadasuke Tsukiyama[6], Terry P. Yamaguchi[7], Walter Birchmeier[8], Shigeaki Kato[9] and Gen Yamada[1,2,*]

β-catenin signaling is one of the key factors regulating the fate of hair follicles (HFs). To elucidate the regulatory mechanism of embryonic HF fate determination during epidermal development/differentiation, we analyzed conditional mutant mice with keratinocytes expressing constitutively active β-catenin (K5-Cre Catnb$^{(ex3)fl/+}$). The mutant mice developed scaly skin with a thickened epidermis and showed impaired epidermal stratification. The hair shaft keratins were broadly expressed in the epidermis but there was no expression of the terminal differentiation markers K1 and loricrin. Hair placode markers (*Bmp2* and *Shh*) and follicular dermal condensate markers (noggin, patched 1 and *Pdgfra*) were expressed throughout the epidermis and the upper dermis, respectively. These results indicate that the embryonic epidermal keratinocytes have switched extensively to the HF fate. A series of genetic studies demonstrated that the epidermal switching to HF fate was suppressed by introducing the conditional mutation K5-Cre Catnb$^{(ex3)fl/+}$Shh$^{fl/-}$ (with additional mutation of Shh signaling) or K5-Cre Catnb$^{(ex3)fl/+}$BmprIA$^{fl/fl}$ (with additional mutation of Bmp signaling). These results demonstrate that Wnt/β-catenin signaling relayed through Shh and Bmp signals is the principal regulatory mechanism underlying the HF cell fate change. Assessment of *Bmp2* promoter activities suggested a putative regulation by β-catenin signaling relayed by Shh signaling towards Bmp2. We also found that Shh protein expression was increased and expanded in the epidermis of K5-Cre Catnb$^{(ex3)fl/+}$BmprIA$^{fl/fl}$ mice. These results indicate the presence of growth factor signal cross-talk involving β-catenin signaling, which regulates the HF fate.

KEY WORDS: Skin, Hair follicle (HF), Wnt, β-catenin, Bmp, Shh, Cell fate

INTRODUCTION

Recent studies have implicated members of the Wnt/β-catenin signaling pathway as vital regulators of the epithelial-mesenchymal interactions that specify the development of hair follicles (HFs) (Fuchs, 2007; Yu et al., 2008). The essential role of Wnt/β-catenin signaling during HF morphogenesis has been suggested by transgenic and knockout mouse studies (Andl et al., 2002; Gat et al., 1998; Huelsken et al., 2001; Lo Celso et al., 2004). Recent studies using embryos have revealed that embryonic HF fate change, HF differentiation and its excessive induction are induced by stabilized β-catenin (Narhi et al., 2008; Zhang et al., 2008).

Besides Wnt/β-catenin signaling, Bmp (bone morphogenetic protein) and Shh (sonic hedgehog) signaling have also been suggested to regulate HF formation. Bmp signaling has been suggested to regulate HF induction and the patterning of follicles within the skin by repressing the placode fate (Botchkarev et al., 1999; Jamora et al., 2003; Jiang et al., 1999; Noramly and Morgan, 1998; Rendl et al., 2008). Shh signaling regulates HF cell proliferation and morphogenesis (Chiang et al., 1999; St-Jacques et al., 1998). However, the mechanisms involved in the downstream effects of Wnt/β-catenin signaling to regulate HF fate are poorly understood.

To elucidate whether the embryonic HF fate change is regulated by several growth factor signaling pathways associated with Wnt/β-catenin signaling, a conditional cutaneous-specific recombination strategy was employed using a stabilized β-catenin allele, i.e. a β-catenin gene with exon 3 encoding serine and threonine residues flanked by LoxP sites [β-catenin flox(ex3); hereafter designated as Catnb$^{(ex3)fl/+}$]. Cre recombinase-mediated excision leads to the expression of a stabilized, constitutively active form of β-catenin (Harada et al., 1999). We observed that hair placodes and the dermal condensate expanded and that embryonic epidermal keratinocytes displayed an HF-like differentiation in K5-Cre Catnb$^{(ex3)fl/+}$ mutant mice. Intriguingly, those phenotypes were suppressed by introducing an additional conditional mutation: K5-Cre Catnb$^{(ex3)fl/+}$BmprIA$^{fl/fl}$ or K5-Cre Catnb$^{(ex3)fl/+}$Shh$^{fl/-}$. These results demonstrate that growth factor signal cross-talk under conditions of activated β-catenin are mediated through Shh and Bmp signaling, and are the principal mechanisms for regulating HF fate. The assessment of the Bmp(s) promoter activity and analysis of Shh protein expression also provided clues to understand the mechanisms of signal cross-talk during embryonic HF fate change.

MATERIALS AND METHODS

Mouse mutant alleles

The Catnb$^{(ex3)fl/+}$, BmprIA$^{fl/fl}$, Shh$^{fl/fl}$ and Shh$^{fl/-}$ alleles, and the keratin 5-Cre (K5-Cre) strain have been described previously (Chiang et al., 1996; Harada et al., 1999; Mishina et al., 2002; Tarutani et al., 1997) (Jackson Laboratories Stock #004293). The BAT-*lacZ* mouse containing a construct including the Tcf/Lef-binding sites has also been described (Nakaya et al., 2005). Sampling of dorsal skin specimens was performed

[1]Center for Animal Resources and Development (CARD), and [2]Global COE 'Cell Fate Regulation Research and Education Unit', Kumamoto University, Kumamoto 860-0811, Japan. [3]Department of Geriatric and Environmental Dermatology, Nagoya City University Graduate School of Medical Sciences, Nagoya 467-8601, Japan. [4]Department of Dermatology, Hokkaido University Graduate School of Medicine, Sapporo 060-8638, Japan. [5]Department of Pharmacology, Graduate School of Medicine, Kyoto University, Kyoto 606-8501, Japan. [6]Department of Molecular Biochemistry, Hokkaido University, Sapporo, Hokkaido 060-8638, Japan. [7]Cancer and Developmental Biology Laboratory, National Cancer Institute-Frederick, NIH Frederick, MD 21702, USA. [8]Department of Cancer Biology, Max-Delbrück-Center for Molecular Medicine, 13125 Berlin, Germany. [9]Institute of Molecular and Cellular Biosciences, University of Tokyo, Tokyo 113-0032, Japan.

*Author for correspondence (e-mail: gensan@gpo.kumamoto-u.ac.jp)

Accepted 17 November 2008

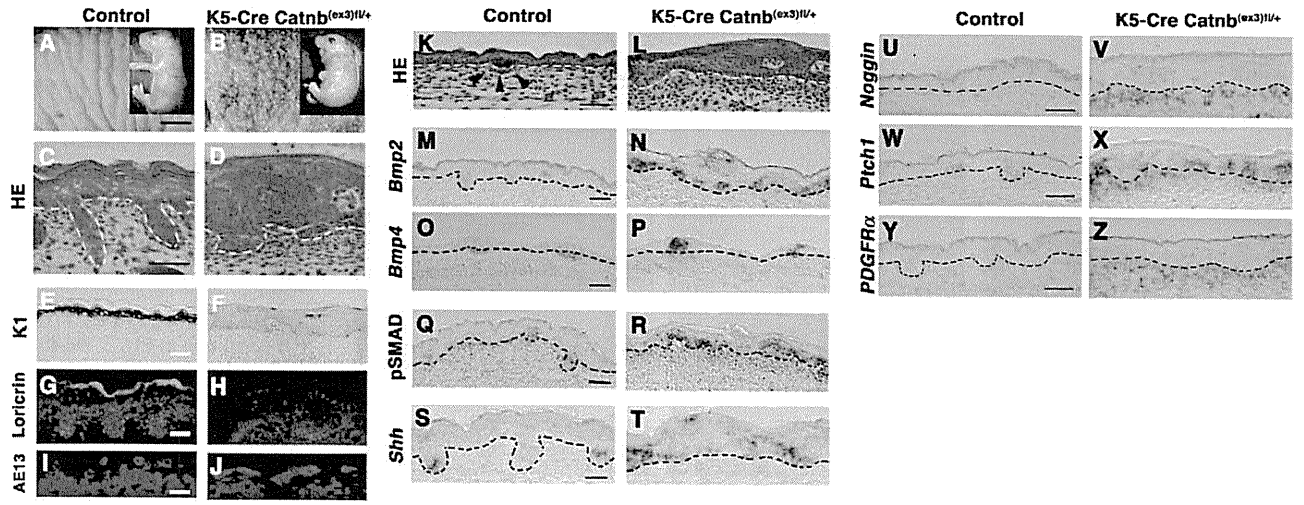

Fig. 1. Switching of embryonic epidermal keratinocytes to HF fate in K5-Cre Catnb$^{(ex3)fl/+}$ mutant skin. (**A**,**B**) Gross appearance of control and of K5-Cre Catnb$^{(ex3)fl/+}$ mutant skin at E18.5. (**C**,**D**) Histology of control and of K5-Cre Catnb$^{(ex3)fl/+}$ mutant skin at E18.5. (**E-H**) Epidermal differentiation marker expression: K1 (brown) and loricrin (green) at E18.5. (**I**,**J**) Immunostaining with AE13 antibody to detect hair shaft keratins (red) at E18.5. (**K**,**L**) Histological alteration of the K5-Cre Catnb$^{(ex3)fl/+}$ mutant dermis compared with control, showing the dermal condensate throughout the upper dermis. Arrowheads in K indicate dermal condensate. (**M**,**N**) *Bmp2* expression is broadly induced in K5-Cre Catnb$^{(ex3)fl/+}$ mutant epidermis at E16.5. (**O**,**P**) *Bmp4* expression is ectopically detected in the mutant epidermis at E15.0. (**Q**,**R**) The pSMAD level is prominently increased in the mutant epidermis and dermis compared with the control. (**S**,**T**) *Shh* expression is broadly detected in the mutant epidermis at E18.5. (**U-Z**) The dermal condensate markers noggin, *Ptch1* and *Pdgfra* are expressed throughout the upper dermis in K5-Cre Catnb$^{(ex3)fl/+}$ skin at E16.5. Dashed lines indicate the dermal-epithelial border. Scale bars: 1 mm for A,B; 50 μm for C-J,M-R; 25 μm for K,L,S-Z.

between embryonic day (E) 10.5 and E18.5. All animal experiments were approved by the Animal Study Committee of the Kumamoto University School of Medicine.

Histology, immunohistochemistry and X-gal staining analysis

The gross skin phenotype images were captured using the VHX system (Keyence). Embryonic dorsal skin specimens were fixed overnight in 4% paraformaldehyde (PFA)/PBS, dehydrated in methanol and embedded in paraffin. Serial sections (6 μm) were prepared for Hematoxylin and Eosin (HE) staining and immunohistochemistry.

Antibodies used were: keratin 1 (Covance PRB-165P), AE13 (AbCam), loricrin (Covance PRB-145P), β-catenin (BD Bioscience), Ki67 (Novo Castra), Shh (Santa Cruz H-160) and pSmad1/5/8 (Cell Signaling) (Ahn et al., 2001). Secondary antibodies were conjugated to Alexa Fluor 488 or 546 IgGs (Molecular Probes/Invitrogen). X-gal staining was performed as described previously (Haraguchi et al., 2007).

In situ hybridization for gene expression analysis

In situ hybridization analysis was performed on 8-μm paraffin sections of embryonic back skin (Suzuki et al., 2008) with probes for *Bmp2*, *Shh*, *Lef1*, *Dkk1*, *Msx2* and *Pdgfra* (kindly provided by B. L. Hogan, C. Shukunami, H. Clevers, U. Rüther, Y. Liu and P. Soriano, respectively), *Ptch1* (Goodrich et al., 1996), *Bmp4* (Jones et al., 1991) and noggin (McMahon et al., 1998). The *Wnt10b* probe was generated by PCR using the following primers (F, 5′-GCG GGT CTC CTG TTC TTG GC-3′; R, 5′-AGA GGC GGC TGG TCT TGT TG-3′).

Promoter assay with luciferase reporter activity

Bmp2 and *Bmp4* promoter reporter constructs contain murine gene fragments of 1725 bp (–410 to +1315) and 1828 bp (–1402 to +426), respectively, in the reporter gene plasmid pGL3 basic (Invitrogen); numbers are relative to the transcriptional start site. HaCaT cells were plated into 24-well plates at 2×10^5 cells per well in DMEM/10% FBS 24 hours prior to transfection. The reporter plasmids were co-transfected with a control vector or with pcDNA3.1-His-mouse Gli2-delN2 (N-terminally truncated Gli2 as a strong activator for hedgehog signaling) (Sasaki et al., 1999), using the TransFast Transfection Reagent (Promega), and luciferase activity was measured using a Dual Luciferase Assay Kit (Promega) (Nishida et al., 2008).

RESULTS AND DISCUSSION

Augmented β-catenin switches embryonic epidermal keratinocytes to the HF fate

To examine whether embryonic HF fate is determined through signaling pathways regulated by β-catenin, conditional epidermal modulation of β-catenin signaling was employed. Keratin 5-Cre (K5-Cre)-mediated recombination and the expression kinetics of the constitutively active β-catenin in the developing skin epidermis are shown in Fig. S1 in the supplementary material.

K5-Cre Catnb$^{(ex3)fl/+}$ mutant mice displayed scaly skin with pillar-shaped comedo-like white spots in the embryonic epidermis (Fig. 1B). Histological analyses of the mutant embryos demonstrated a thickened epidermis without the granular layers at E18.5 (Fig. 1C,D; the kinetics of the morphological alterations are shown in Fig. S2 in the supplementary material). In addition, the mutant skin also showed abnormal epidermal differentiation and denser cell layers in the upper dermis (Fig. 1D). Interestingly, the mutant epidermis showed follicular keratinization with morphological trichilemma-type structures (see Fig. S3 in the supplementary material). To determine the degree of such structural changes, we analyzed the expression of terminal differentiation markers [K1 (Krt1 – Mouse Genome Informatics) and loricrin] and hair shaft keratins that are specifically recognized by the AE13 antibody (Lynch et al., 1986). Expression of K1 and loricrin was dramatically reduced in K5-Cre Catnb$^{(ex3)fl/+}$ skin at E18.5 (Fig. 1E-H). By contrast, hair shaft keratins were expressed broadly and strongly in the K5-Cre Catnb$^{(ex3)fl/+}$ mutant epidermis at E18.5, suggesting that augmented β-catenin signaling induces HF-like differentiation (Fig. 1E-J; the expression kinetics are shown in Fig. S4 in the supplementary material).

Embryonic HF morphogenesis is governed by epithelial-mesenchymal interactions between keratinocytes in the hair placode and fibroblasts in the mesenchymal condensate (Hardy, 1992; Oro and Scott, 1998; Sengel, 1976). Signals from the hair placode induced the underlying mesenchymal cells to condense (dermal

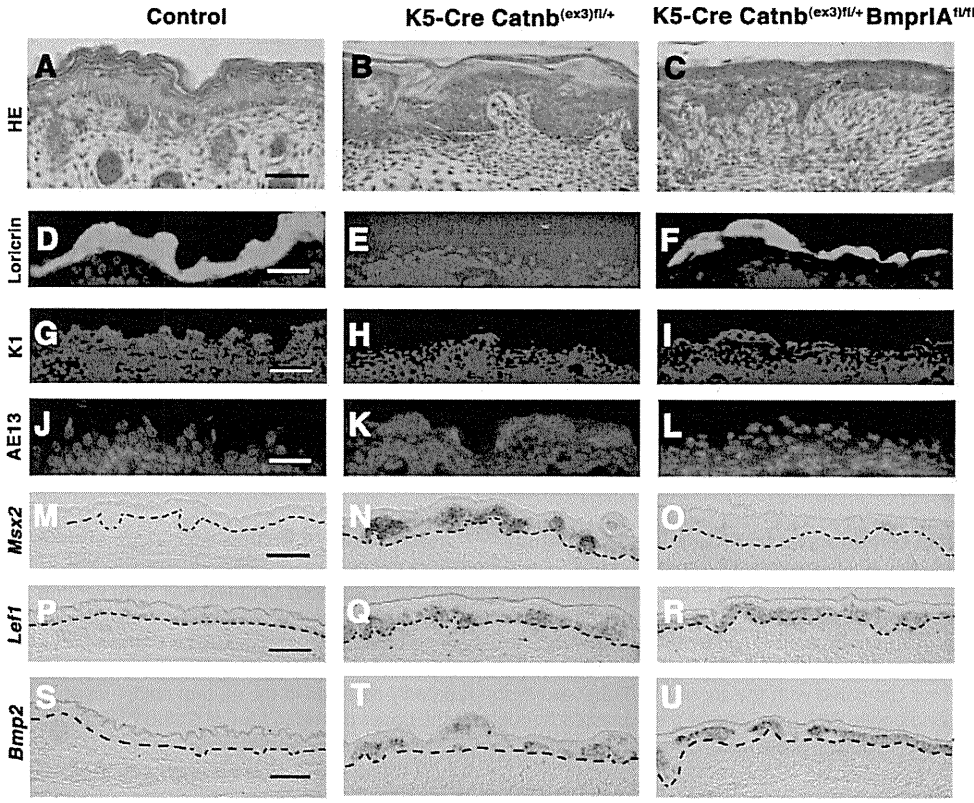

Fig. 2. The loss of Bmp signaling in the epidermis restores the K5-Cre Catnb$^{(ex3)fl/+}$ mutant HF-like differentiation.
(**A-C**) Histological analysis of control, K5-Cre Catnb$^{(ex3)fl/+}$ and double mutant skin at E18.5. (**D-L**) The restoration of loricrin (green) and K1 (red) expression, and the suppression of expression of hair shaft keratins recognized by AE13 antibody (red), in double mutant skin at E18.5. (**M-R**) In situ hybridization for *Msx2* and *Lef1* expression at E16.5. (**S-U**) Upon induction, expression of hair placode marker gene *Bmp2* remained in the K5-Cre Catnb$^{(ex3)fl/+}$ BmprIA$^{fl/fl}$ mutant epidermis. Dashed lines indicate the dermal-epithelial border. Scale bars: 50 μm for A-L; 100 μm for M-U.

condensate; Fig. 1K; arrowheads). K5-Cre Catnb$^{(ex3)fl/+}$ mutant skin showed such dermal condensates throughout the upper dermis at E16.5 (Fig. 1L, the kinetics of these morphological changes are shown in Fig. S2 in the supplementary material). To further analyze the basis of the excessive induction of HFs, the expression of hair placode markers (Bmps and *Shh*) and dermal condensate markers [noggin, patched 1 (*Ptch1*) and *Pdgfra*] was examined. *Bmp2* and *Bmp4* are expressed in the hair placode and in the underlying mesenchymal condensate, respectively, in control skin (Fig. 1M,O). *Bmp2* expression was increased broadly in the mutant epidermis at E16.5 (Fig. 1N). *Bmp4* expression was localized ectopically in the mutant epidermis at E15.0 with expanded expression in later stages (Fig. 1P; data not shown). To investigate the extent of Bmp signaling, the pSMAD levels were analyzed and were significantly increased in the mutant epidermis and in the underlying mesenchyme compared with the control at E16.5 (Fig. 1Q,R; see also Fig. S5 in the supplementary material). *Shh* expression was also broadly detected in the mutant epidermis at E18.5 (Fig. 1T). The induced expression of *Bmp2*, *Bmp4*, pSMAD, *Shh* and *Wnt10b* (another early placode marker) was already observed at E11.5 (see Figs S5, S6 in the supplementary material). Dermal condensate markers were expressed throughout the upper dermis in K5-Cre Catnb$^{(ex3)fl/+}$ mutant mice at E16.5 (Fig. 1U-Z). These results suggest that augmented β-catenin signaling induces the excessive HF induction and HF-like differentiation, leading to an HF fate.

Suppression of HF-like differentiation by the conditional mutation of K5-Cre Catnb$^{(ex3)fl/+}$BmprIA$^{fl/fl}$

To investigate the potential effect of the increased Bmp signaling in K5-Cre Catnb$^{(ex3)fl/+}$ mutant mice, a conditional double mutant (K5-Cre Catnb$^{(ex3)fl/+}$BmprIA$^{fl/fl}$) was examined. BmprIA (Bmpr1a – Mouse Genome Informatics) is a type I Bmp receptor and its signaling is essential for hair shaft differentiation (Yuhki et al., 2004). The HF-like epidermal differentiation observed in K5-Cre Catnb$^{(ex3)fl/+}$ mutant mice was suppressed by introduction of the double mutation at E18.5 (Fig. 2A-L). Loricrin and K1 expression were restored (Fig. 2E,F,H,I). In addition, the augmented AE13 epitope reactivity observed in K5-Cre Catnb$^{(ex3)fl/+}$ mutants was suppressed in the double mutants, confirming the dramatic suppression of HF-like differentiation (Fig. 2K,L). *Msx2* is one of the downstream target genes of Bmp signaling and regulates the expression of *Foxn1*, which controls the transcription of hair keratin genes (Ma et al., 2003; Meier et al., 1999). The expression of *Msx2* was dramatically upregulated in K5-Cre Catnb$^{(ex3)fl/+}$ mutant epidermis, whereas its expression suppressed in the double mutants at E16.5 (Fig. 2N,O). The Wnt/β-catenin pathway transcriptional effector Lef1 regulates differentiation of the hair shaft (Merrill et al., 2001). Its increased expression was maintained in the double mutant epidermis at E16.5 (Fig. 2Q,R). We also found that the region with the induced hair placode marker gene expression, which includes that of *Bmp2*, remained in the K5-Cre Catnb$^{(ex3)fl/+}$BmprIA$^{fl/fl}$ mutant epidermis (Fig. 2T,U; data not shown). These results indicate that the pathway in which β-catenin is relayed by Bmp signaling plays a principal role in inducing HF-like differentiation, but not in the excessive induction of HFs (Fig. 4H).

Suppression of excessive HF induction by the conditional mutation of K5-Cre Catnb$^{(ex3)fl/+}$Shh$^{fl/-}$

One of the prominent phenotypes caused by augmented β-catenin is aberrant HF patterning, the excessive hair placode induction with the underlying dermal condensate (Fig. 1) (Narhi et al., 2008; Zhang et al., 2008). The excessive induction of HFs was not suppressed in K5-Cre Cantb$^{(ex3)fl/+}$BmprIA$^{fl/fl}$ mutant skin (Fig. 2T,U).

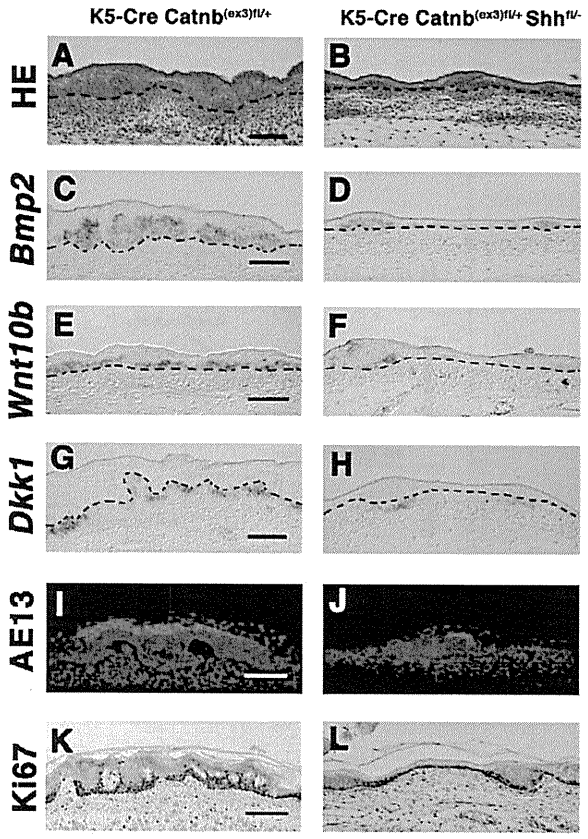

Fig. 3. The involvement of Shh signaling as a crucial downstream effector of β-catenin signaling for the excessive HF induction. (**A**,**B**) Suppression of excessive HF induction in the double conditional mutant K5-Cre Catnb$^{(ex3)fl/+}$Shh$^{fl/-}$ at E16.5. (**C-J**) Suppression of induced *Bmp2*, *Wnt10b* and *Dkk1* expression, and of AE13 antibody staining (red), in the double mutant skin at E16.5. (**K**,**L**) Cell proliferation analysis using Ki67 antibody at E18.5. Cell proliferation is increased in K5-Cre Catnb$^{(ex3)fl/+}$ mutant (K) and is suppressed in K5-Cre Cantb$^{(ex3)fl/+}$Shh$^{fl/-}$ double mutant (L) epidermis. Dashed lines indicate the dermal-epithelial border. Scale bars: 50 μm for A-L.

Shh controls cell proliferation and formation of the dermal papilla (Fuchs, 2007; Millar, 2002; Schmidt-Ullrich and Paus, 2005). Its overexpression leads to the induction of dermal condensate during feather formation (Ting-Berreth and Chuong, 1996) and its inhibition impairs dermal papilla formation (Nanba et al., 2003). Shh has been suggested to be regulated by the β-catenin signaling pathway (Huelsken et al., 2001; Zhang et al., 2008). Indeed, expression of *Shh* was increased in the skin of K5-Cre Cantb$^{(ex3)fl/+}$ mice (Fig. 1T). To elucidate whether the excessive induction of HFs is mediated by the Shh signaling pathway associated with augmented β-catenin signaling, we analyzed K5-Cre Cantb$^{(ex3)fl/+}$Shh$^{fl/-}$ double mutant skin. Shh signaling was indeed decreased in K5-Cre Cantb$^{(ex3)fl/+}$Shh$^{fl/-}$ skin based on reduced *Ptch1* expression at E14.5 (see Fig. S7 in the supplementary material). The number of hair placodes was increased in the K5-Cre Catnb$^{(ex3)fl/+}$ epidermis, spreading from the early-induced hair placodes (Fig. S2 in the supplementary material; data not shown). The excessive induction of HFs was suppressed in the double mutant skin based on reduced hair placode marker gene expression (*Bmp2* and *Wnt10b*) and reduced *Dkk1* expression at E16.5 (Fig. 3A-H). The expression of *Dkk1* is elevated in the dermis at sites of placode development in normal embryos (Andl et al., 2002). *Dkk1* expression was strongly induced in the K5-Cre Catnb$^{(ex3)fl/+}$ dermis, but its expression was significantly decreased in K5-Cre Cantb$^{(ex3)fl/+}$Shh$^{fl/-}$ skin throughout the upper dermis at E16.5 (Fig. 3H). The increased expression of dermal condensate markers (noggin and *Pdgfra*) was also suppressed in K5-Cre Cantb$^{(ex3)fl/+}$Shh$^{fl/-}$ skin (data not shown). Furthermore, the induction of HF-like differentiation was suppressed in the K5-Cre Cantb$^{(ex3)fl/+}$Shh$^{fl/-}$ mutant based on the reduced immunostaining observed for AE13 at E16.5 (Fig. 3I,J). We also observed decreased epidermal cell proliferation in K5-Cre Cantb$^{(ex3)fl/+}$Shh$^{fl/-}$ mutants compared with K5-Cre Catnb$^{(ex3)fl/+}$ mice at E18.5 (Fig. 3K,L). These results suggested that Shh signaling is a crucial downstream pathway of β-catenin signaling for the excessive induction of HFs with increased cell proliferation (Fig. 4H).

Wnt/β-catenin signaling may also be one of the genetic upstream pathways of Bmp during embryonic HF development (Huelsken et al., 2001; Narhi et al., 2008). The intensity of pSMAD staining in K5-Cre Cantb$^{(ex3)fl/+}$ mutant skin was suppressed in both the epidermis and the mesenchyme of K5-Cre Cantb$^{(ex3)fl/+}$Shh$^{fl/-}$ mutant skin at E16.5 (Fig. 4C, brackets). As for the regulatory mechanisms controlling Bmp expression, we found several candidate Lef/Tcf-binding sites in the 1.8-kb *Bmp4* promoter and several GLI-binding sites in the 1.7-kb *Bmp2* promoter using rVISTA bioinformatics analysis (Fig. 4D, yellow boxes; data not shown). Transient promoter assays showed that the *Bmp4* promoter was not regulated through stabilized β-catenin signaling under the current experimental conditions (data not shown), but revealed an increase of *Bmp2* promoter activity caused by Gli2 in vitro (Fig. 4D). In fact, the current double mutant analyses on K5-Cre Catnb$^{(ex3)fl/+}$Shh$^{fl/-}$ skin showed suppression of the increased *Bmp2* expression, suggesting that the regulation of Bmp signaling through Shh signaling is an essential molecular mechanism for the HF fate change (Fig. 3C,D). Increased *Bmp2* expression, the intensity of pSMAD staining and AE13 immunostaining remained in early-induced HFs of the K5-Cre Catnb$^{(ex3)fl/+}$Shh$^{fl/-}$ epidermis (Fig. 3; Fig. 4C, outside of the brackets). It has been shown that Shh signaling is not required for the initiation of HF formation and that HF differentiation is not inhibited in Shh mutant skin (Chiang et al., 1999; St-Jacques et al., 1998). Our current study indicates that Shh signaling is required for the expansion of hair follicle fate by augmented β-catenin signaling, although it is not required for either the initial specification of hair placodes or the differentiation of early-induced HFs.

The regulation of HF space has been considered to be controlled by diffusible molecules that either promote or repress follicular fate (Jiang et al., 2004; Mikkola and Millar, 2006; Millar, 2002). Previously, it was shown that Shh is one of the placode activators, while Bmps are generally regarded as being placode inhibitors that mediate lateral inhibition, which is known as the reaction-diffusion mechanism (Jung et al., 1998). Studies on chick embryonic skin suggested that Shh induces the expression of Bmps, whereas Bmps suppress *Shh* expression during feather development (Harris et al., 2005; Jung et al., 1998). We further analyzed the expression of Shh protein in K5-Cre Cantb$^{(ex3)fl/+}$BmprIA$^{fl/fl}$ skin. Interestingly, Shh protein expression was both increased and expanded in K5-Cre Cantb$^{(ex3)fl/+}$BmprIA$^{fl/fl}$ mutant epidermis at E16.5 (Fig. 4E-G).

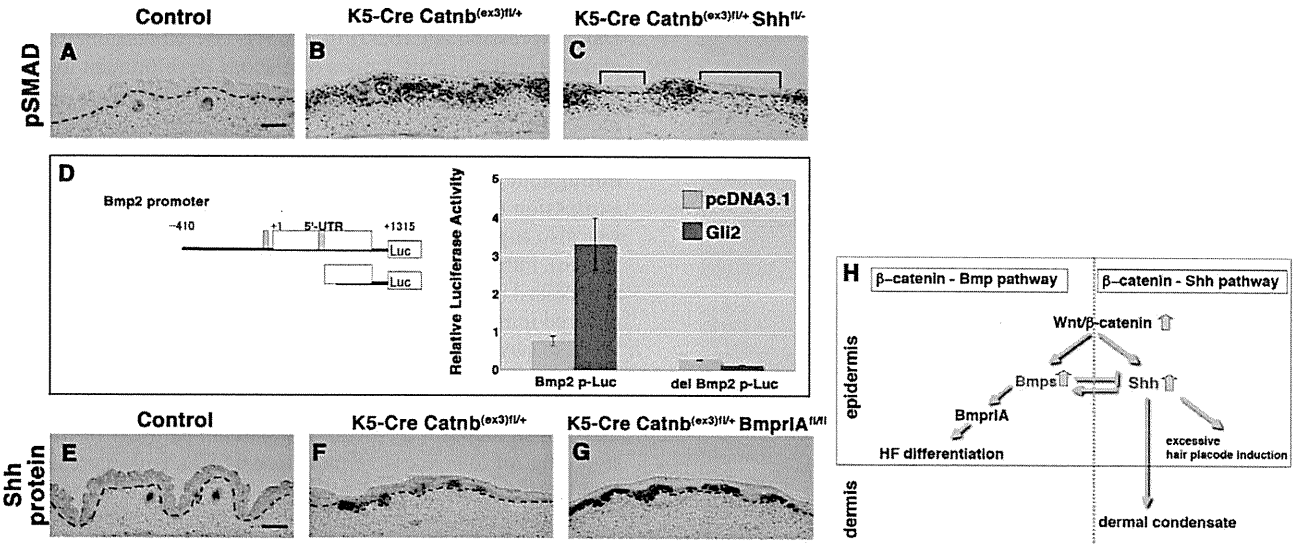

Fig. 4. A possible regulatory mechanism between Shh and Bmp signaling that underlies Wnt/β-catenin signaling pathway. (**A-C**) The intensity of pSMAD staining in K5-Cre Cantb$^{(ex3)fl/+}$ is suppressed both in the epidermis and the mesenchyme of K5-Cre Cantb$^{(ex3)fl/+}$Shh$^{fl/-}$ skin at E16.5 (C, brackets). Such intense pSMAD staining remains in early-induced HFs (outside of the brackets). (**D**) Activation of the *Bmp2* promoter (Bmp2 p-Luc) by introducing the activated Gli2 expression vector; the activation is diminished by deleting the two putative GLI-binding sites (yellow boxes; del Bmp2 p-Luc). (**E-G**) Shh protein expression is increased and expanded in K5-Cre Cantb$^{(ex3)fl/+}$BmprIA$^{fl/fl}$ mutant epidermis at E16.5. (**H**) Schematic of the growth factor network regulating HF fate change. Scale bars: 50 μm for A-C,E-G.

Taken together, the current results are in agreement with the reaction-diffusion mechanism, via the cross-talk between the activator (Shh signaling) and the inhibitor (Bmp signaling) implicated in the periodic patterning of HFs (Fig. 4H) (Jiang et al., 2004; Jung et al., 1998).

We thank Drs Richard Behringer, Yuji Mishina, Brian Crenshaw, Junji Takeda, Cheng-Ming Chuong, Alex Joyner, Hiroshi Sasaki, Chi-Chung Hui, Brandon Wainwright, Anne M. Moon, Vincent J. Hearing, Shinji Takada, Pierre Chambon, Shinichi Miyagawa, Sawako Fujikawa, Shiho Miyaji, Yukiko Ogino, Ryuma Haraguchi, Liqing Liu and Ichiro Katayama for encouragement and suggestions. This study was supported by a Grant-in-Aid for Scientific Research on Priority Areas, General Promotion of Cancer Research in Japan; a Grant-in-Aid for Scientific Research on Priority Areas, Mechanisms of Sex Differentiation; a Grant-in-Aid for Scientific Research (B) and for Young Scientists (B); the Global COE 'Cell Fate Regulation Research and Education Unit'; and a Grant for Child Health and Development from the Ministry of Health, Labour and Welfare, Japan. Deposited in PMC for release after 12 months.

Supplementary material

Supplementary material for this article is available at
http://dev.biologists.org/cgi/content/full/136/3/367/DC1

References

Ahn, K., Mishina, Y., Hanks, M. C., Behringer, R. R. and Crenshaw, E. B., 3rd (2001). BMPR-IA signaling is required for the formation of the apical ectodermal ridge and dorsal-ventral patterning of the limb. *Development* **128**, 4449-4461.

Andl, T., Reddy, S. T., Gaddapara, T. and Millar, S. E. (2002). WNT signals are required for the initiation of hair follicle development. *Dev. Cell* **2**, 643-653.

Botchkarev, V. A., Botchkareva, N. V., Roth, W., Nakamura, M., Chen, L. H., Herzog, W., Lindner, G., McMahon, J. A., Peters, C., Lauster, R. et al. (1999). Noggin is a mesenchymally derived stimulator of hair-follicle induction. *Nat. Cell Biol.* **1**, 158-164.

Chiang, C., Litingtung, Y., Lee, E., Young, K. E., Corden, J. L., Westphal, H. and Beachy, P. A. (1996). Cyclopia and defective axial patterning in mice lacking Sonic hedgehog gene function. *Nature* **383**, 407-413.

Chiang, C., Swan, R. Z., Grachtchouk, M., Bolinger, M., Litingtung, Y., Robertson, E. K., Cooper, M. K., Gaffield, W., Westphal, H., Beachy, P. A. et al. (1999). Essential role for Sonic hedgehog during hair follicle morphogenesis. *Dev. Biol.* **205**, 1-9.

Fuchs, E. (2007). Scratching the surface of skin development. *Nature* **445**, 834-842.

Gat, U., DasGupta, R., Degenstein, L. and Fuchs, E. (1998). De novo hair follicle morphogenesis and hair tumors in mice expressing a truncated beta-catenin in skin. *Cell* **95**, 605-614.

Goodrich, L. V., Johnson, R. L., Milenkovic, L., McMahon, J. A. and Scott, M. P. (1996). Conservation of the hedgehog/patched signaling pathway from flies to mice: induction of a mouse patched gene by Hedgehog. *Genes Dev.* **10**, 301-312.

Harada, N., Tamai, Y., Ishikawa, T., Sauer, B., Takaku, K., Oshima, M. and Taketo, M. M. (1999). Intestinal polyposis in mice with a dominant stable mutation of the beta-catenin gene. *EMBO J.* **18**, 5931-5942.

Haraguchi, R., Motoyama, J., Sasaki, H., Satoh, Y., Miyagawa, S., Nakagata, N., Moon, A. and Yamada, G. (2007). Molecular analysis of coordinated bladder and urogenital organ formation by Hedgehog signaling. *Development* **134**, 525-533.

Hardy, M. H. (1992). The secret life of the hair follicle. *Trends Genet.* **8**, 55-61.

Harris, M. P., Williamson, S., Fallon, J. F., Meinhardt, H. and Prum, R. O. (2005). Molecular evidence for an activator-inhibitor mechanism in development of embryonic feather branching. *Proc. Natl. Acad. Sci. USA* **102**, 11734-11739.

Huelsken, J., Vogel, R., Erdmann, B., Cotsarelis, G. and Birchmeier, W. (2001). beta-Catenin controls hair follicle morphogenesis and stem cell differentiation in the skin. *Cell* **105**, 533-545.

Jamora, C., DasGupta, R., Kocieniewski, P. and Fuchs, E. (2003). Links between signal transduction, transcription and adhesion in epithelial bud development. *Nature* **422**, 317-322.

Jiang, T. X., Jung, H. S., Widelitz, R. B. and Chuong, C. M. (1999). Self-organization of periodic patterns by dissociated feather mesenchymal cells and the regulation of size, number and spacing of primordia. *Development* **126**, 4997-5009.

Jiang, T. X., Widelitz, R. B., Shen, W. M., Will, P., Wu, D. Y., Lin, C. M., Jung, H. S. and Chuong, C. M. (2004). Integument pattern formation involves genetic and epigenetic controls: feather arrays simulated by digital hormone models. *Int. J. Dev. Biol.* **48**, 117-135.

Jones, C. M., Lyons, K. M. and Hogan, B. L. (1991). Involvement of Bone Morphogenetic Protein-4 (BMP-4) and Vgr-1 in morphogenesis and neurogenesis in the mouse. *Development* **111**, 531-542.

Jung, H. S., Francis-West, P. H., Widelitz, R. B., Jiang, T. X., Ting-Berreth, S., Tickle, C., Wolpert, L. and Chuong, C. M. (1998). Local inhibitory action of BMPs and their relationships with activators in feather formation: implications for periodic patterning. *Dev. Biol.* **196**, 11-23.

Lo Celso, C., Prowse, D. M. and Watt, F. M. (2004). Transient activation of beta-catenin signalling in adult mouse epidermis is sufficient to induce new hair follicles but continuous activation is required to maintain hair follicle tumours. *Development* **131**, 1787-1799.